Article

Cell Reports

Control of Smc Coiled Coil Architecture by the ATPase Heads Facilitates Targeting to Chromosomal ParB/*parS* and Release onto Flanking DNA

Graphical Abstract

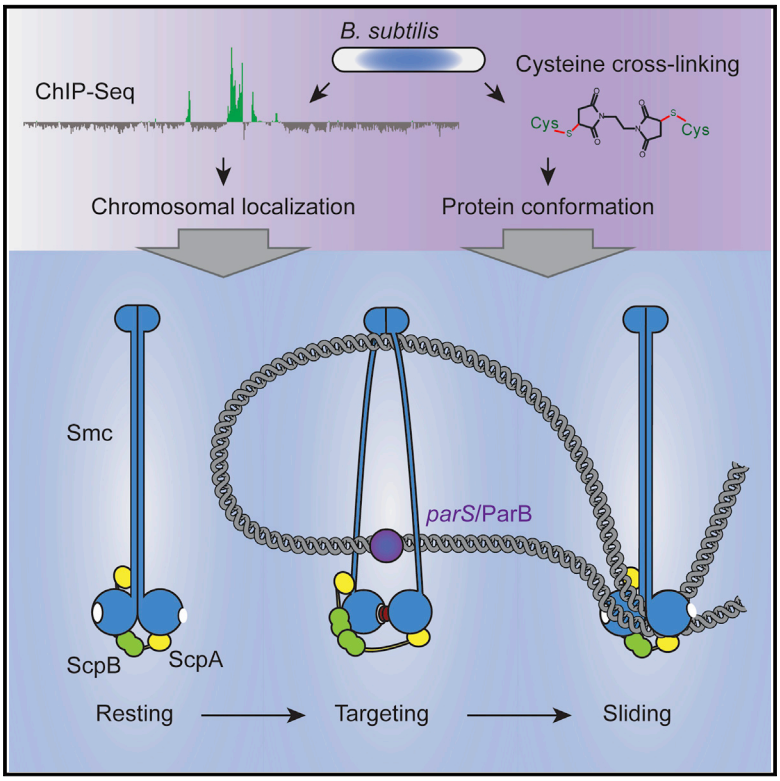

Authors

Anita Minnen, Frank Bürmann, Larissa Wilhelm, Anna Anchimiuk, Marie-Laure Diebold-Durand, Stephan Gruber

Correspondence

sgruber@biochem.mpg.de

In Brief

Smc/ScpAB is an important chromosome-organizing machine in bacteria. Minnen et al. show that targeting of Smc/ScpAB to chromosomal *parS*/ParB sites requires ATP-dependent engagement of Smc heads, which promotes disengagement of the Smc coiled coils and drives the complex into a targeting-competent open conformation.

Highlights

- ATP-dependent head engagement is required for chromosomal targeting of Smc/ScpAB
- ATP-dependent head engagement drives coiled-coil opening of Smc in vivo
- Targeting of Smc/ScpAB to *parS*/ParB requires the head-proximal coiled coil of Smc
- Hinge dimerization antagonizes head engagement, coiled-coil opening, and targeting

Accession Numbers

GSE76949

Minnen et al., 2016, Cell Reports *14*, 1–14
March 1, 2016
http://dx.doi.org/10.1016/j.celrep.2016.01.066

CellPress

Please cite this article in press as: Minnen et al., Control of Smc Coiled Coil Architecture by the ATPase Heads Facilitates Targeting to Chromosomal ParB/*parS* and Release onto Flanking DNA, Cell Reports (2016), http://dx.doi.org/10.1016/j.celrep.2016.01.066

Cell Reports
Article

Control of Smc Coiled Coil Architecture by the ATPase Heads Facilitates Targeting to Chromosomal ParB/*parS* and Release onto Flanking DNA

Anita Minnen,[1,2] Frank Bürmann,[1,2] Larissa Wilhelm,[1] Anna Anchimiuk,[1] Marie-Laure Diebold-Durand,[1] and Stephan Gruber[1,*]
[1]Research Group 'Chromosome Organization and Dynamics', Max Planck Institute of Biochemistry, Am Klopferspitz 18, 82152 Martinsried, Germany
[2]Co-first author
*Correspondence: sgruber@biochem.mpg.de
http://dx.doi.org/10.1016/j.celrep.2016.01.066

SUMMARY

Smc/ScpAB promotes chromosome segregation in prokaryotes, presumably by compacting and resolving nascent sister chromosomes. The underlying mechanisms, however, are poorly understood. Here, we investigate the role of the Smc ATPase activity in the recruitment of Smc/ScpAB to the *Bacillus subtilis* chromosome. We demonstrate that targeting of Smc/ScpAB to ParB/*parS* loading sites is strictly dependent on engagement of Smc head domains and relies on an open organization of the Smc coiled coils. We find that dimerization of the Smc hinge domain stabilizes closed Smc rods and hinders head engagement as well as chromosomal targeting. Conversely, the ScpAB sub-complex promotes head engagement and Smc rod opening and thereby facilitates recruitment of Smc to *parS* sites. Upon ATP hydrolysis, Smc/ScpAB is released from loading sites and relocates within the chromosome—presumably through translocation along DNA double helices. Our findings define an intermediate state in the process of chromosome organization by Smc.

INTRODUCTION

Proper segregation of the genetic material during cell division relies on the organization of replicated DNA molecules into compact and individualized sister chromosomes. In eukaryotes, condensation and resolution of chromatin into morphologically distinct chromatids occurs early in mitosis and depends on the interplay of nucleosomes, DNA topoisomerase II and structural maintenance of chromosomes (SMC) protein complexes such as condensin and cohesin (Houlard et al., 2015; Shintomi et al., 2015). In bacteria, segments of the circular chromosome are sequentially partitioned to opposite halves of the cell in line with their duplication by the two replication forks. Resolution of bacterial chromosomes is thus an ordered process, which initiates near the replication origin and concludes with the separation of the replication terminus region. Prokaryotic SMC complexes, called Smc/ScpAB and MukBEF, are enriched in the vicinity of the replication origin on the bacterial chromosome (Badrinarayanan et al., 2012; Danilova et al., 2007; Gruber and Errington, 2009; Minnen et al., 2011; Sullivan et al., 2009; Wilhelm et al., 2015). In rapidly growing cells of *Bacillus subtilis*, inactivation of Smc/ScpAB is lethal due to a severe block in replication origin separation and nucleoid partitioning (Britton et al., 1998; Gruber et al., 2014; Mascarenhas et al., 2002; Moriya et al., 1998; Soppa et al., 2002; Wang et al., 2014). How Smc/ScpAB enables timely resolution of sister replication origins is largely unclear.

A 50-nm long intramolecular coiled-coil constitutes the central part of SMC proteins, which connects a "hinge" domain with an ATPase "head" domain (Haering et al., 2002; Hirano and Hirano, 2002; Melby et al., 1998). In bacteria, homotypic interaction of two Smc proteins at their hinge supports the alignment of the two Smc coiled coils to produce a highly elongated rod-shaped Smc dimer (Soh et al., 2015). At the hinge-distal end of the Smc rod a single subunit of the kleisin family of proteins (named ScpA in bacteria) binds to the Smc dimer via two separate interfaces (Bürmann et al., 2013; Gruber et al., 2003; Haering et al., 2002; Schleiffer et al., 2003). A helical bundle is formed by ScpA's N-terminal domain and the "neck" coiled coil of one Smc subunit (Bürmann et al., 2013; Gligoris et al., 2014). ScpA's C-terminal winged-helix domain attaches to the "cap" of the head in the other Smc subunit (Bürmann et al., 2013; Haering et al., 2004). Asymmetric tripartite rings made up of one ScpA and two Smc proteins are thus formed. Like its eukaryotic descendants, Smc/ScpAB entraps chromosomal DNA molecules within the confines of its SMC/kleisin ring (Cuylen et al., 2011; Gligoris et al., 2014; Wilhelm et al., 2015). DNA entrapment depends on the ScpB subunit, which forms dimers and associates with a central segment of ScpA, as well as on ATP hydrolysis by the Smc complex (Bürmann et al., 2013; Kamada et al., 2013; Wilhelm et al., 2015).

Smc/ScpAB localizes in foci within the bacterial cell. These Smc protein clusters are generally positioned in the vicinity of a copy of the replication origin in *B. subtilis* and *Streptococcus pneumoniae* (Graumann et al., 1998; Gruber and Errington, 2009; Kleine Borgmann et al., 2013; Minnen et al., 2011; Sullivan

Please cite this article in press as: Minnen et al., Control of Smc Coiled Coil Architecture by the ATPase Heads Facilitates Targeting to Chromosomal ParB/*parS* and Release onto Flanking DNA, Cell Reports (2016), http://dx.doi.org/10.1016/j.celrep.2016.01.066

et al., 2009). Targeting of Smc/ScpAB to the replication origin region and formation of Smc foci relies on ParB protein and *parS* sites. ParB binds to short palindromic *parS* sequences, the six most prominent of which are scattered within a 350 kb region (<10% of the genome) surrounding the replication origin in *B. subtilis*. In several bacteria, the replicating chromosome displays a distinctive "longitudinal" organization within the cell (Le et al., 2013; Marbouty et al., 2014, 2015; Umbarger et al., 2011; Vallet-Gely and Boccard, 2013; Wang et al., 2015): The newly replicated origins are generally found at the outer edges of the elongating chromosome, while other loci on the nascent chromosome are linearly arranged between the replication origin and the more centrally located terminus. Corresponding positions on opposite arms of the chromosome are frequently juxtaposed. The Smc/ScpAB complex as well as ParB protein and *parS* sites are essential for establishing this longitudinal organization of bacterial chromosomes (Le et al., 2013; Marbouty et al., 2015; Umbarger et al., 2011; Wang et al., 2015). How the loading of Smc/ScpAB by ParB/*parS* at few genomic positions governs global chromosome organization, however, is unclear (Bürmann and Gruber, 2015).

The SMC head domains share a common fold with nucleotide binding domains (NBD) found in ABC transporters. These domains undergo cycles of engagement and disengagement driven by ATP binding and ATP hydrolysis. In Smc/ScpAB, the Smc ATPase controls DNA binding to the distant hinge domain (Hirano and Hirano, 2006; Soh et al., 2015). Head engagement appears to promote the dissolution of the Smc coiled coil rod and thereby exposes an otherwise occluded binding site for DNA at the Smc hinge (Soh et al., 2015). If, and how, such a potential ATP-driven conformational transition might be relevant for the ParB-dependent recruitment of Smc/ScpAB toward the replication origin region of the bacterial chromosome is unclear. In yeast, ATP hydrolysis by cohesin has been implicated in its chromosomal relocation from sites occupied by the loading complex. However, the underlying molecular mechanisms remain elusive (Hu et al., 2011).

Here, we show that the Smc ATPase cycle controls the dynamic association of Smc/ScpAB with the bacterial chromosome. It determines the initial targeting of Smc/ScpAB to its chromosomal loading sites and subsequent re-distribution into flanking DNA. Smc head engagement is crucial for the recognition of the ParB/*parS* loading platform. We find that Smc head engagement is remarkably inefficient in Smc/ScpAB, due to the inhibitory action of Smc hinge and Smc rod, which is partially relieved by ScpAB. A head-proximal region of the Smc coiled coil is critical for targeting to ParB/*parS*. An Smc mutant defective in ATP hydrolysis is highly enriched at *parS* sites but fails to localize to other parts of the chromosome, including the neighboring replication origin and distant chromosomal arm loci. Smc appears to be released from loading sites to relocate along DNA to other parts of the chromosome in a manner that requires at least one round of ATP hydrolysis. Overall, our results demonstrate that engagement and disengagement of Smc heads define two distinct modes of chromosome association by Smc/ScpAB. Furthermore, they support the intriguing notion that movement of Smc/ScpAB along chromosome DNA is a critical aspect of its activity, which might be related to DNA loop extrusion by Smc.

RESULTS

Smc ATPase Activity Controls the Dynamic Distribution of Smc/ScpAB over the Bacterial Chromosome

To investigate a potential role of the Smc ATP hydrolysis cycle in the localization of Smc/ScpAB complexes within the bacterial cell and on the bacterial chromosome, we made use of well-characterized, single amino-acid substitutions in the Smc head domain, which specifically block ATP binding (K37I or D1117A) or ATP-dependent head engagement (S1090R), alleviate a proposed stimulatory effect of DNA on ATP hydrolysis (R57A), or strongly reduce Smc ATP hydrolysis (E1118Q; or EQ for short) (Figure 1A) (Hirano et al., 2001; Hirano and Hirano, 2004, 2006; Lammens et al., 2004; Schwartz and Shapiro, 2011). These mutant proteins, with the exception of Smc(R57A), fail to support growth of *B. subtilis* on rich medium indicating that the mutations render the Smc protein non-functional (Figure S1A) (Gruber et al., 2014). All non-functional Smc proteins, however, are expressed to normal levels as judged by immunoblotting using an α-Smc antiserum (Figure 1B) and efficiently bind to the kleisin subunit ScpA (Bürmann et al., 2013; Wilhelm et al., 2015). The *smc* alleles were then tagged at their C terminus with a monomeric version of *gfp* and integrated into the endogenous locus by allelic replacement. Cells were analyzed by fluorescence imaging on minimal medium, which supports near normal growth of *smc* mutant strains. Wild-type Smc-GFP protein formed approximately one GFP focus per μm cell length (Figures 1C and S1H) (Graumann et al., 1998; Gruber and Errington, 2009; Sullivan et al., 2009). The cellular localization of the R57A mutant protein was indistinguishable from wild-type Smc. In contrast, K37I, D1117A, and S1090R mutant proteins failed to form any discernible structures in fluorescence images being indicative of a dispersed cellular localization (Mascarenhas et al., 2005). Crucially, the Smc(EQ) protein produced bright GFP foci, which on average occurred slightly less frequently than in wild-type cells (Figures 1C and S1H). These observations demonstrate the involvement of the Smc ATPase activity in the sub-cellular organization of Smc complexes and indicate that Smc is able to localize within the cell when its ATP hydrolysis activity is reduced but not when ATP binding or Smc head engagement is blocked.

Next, we used untagged alleles of all ATPase mutants to examine their chromosomal distribution in *B. subtilis* by chromatin immunoprecipitation (ChIP) with an antiserum raised against the Smc protein. qPCR with primer pairs specific for selected regions of the chromosome was performed to measure the co-purification of chromosomal DNA with Smc. As predicted from their inability to form GFP foci in the cell, ATP binding and head engagement mutants resulted in little DNA co-purification similar to the Δ*smc* control—being consistent with the notion that ATP binding and engagement mutants fail to localize to the chromosome (Figure 1D). Wild-type Smc produced highly significant ChIP enrichment of origin proximal DNA (*parS-356*, *parS-359*, and *dnaA*) as observed before with tagged alleles of *smc* (Gruber and Errington, 2009). Intriguingly, the Smc(EQ) protein showed on the one hand markedly stronger localization to *parS* DNA than wild-type Smc and on the other hand quite low enrichment at the juxtaposed *dnaA* locus. Clearly, Smc(EQ) protein is able to efficiently target specific regions of the

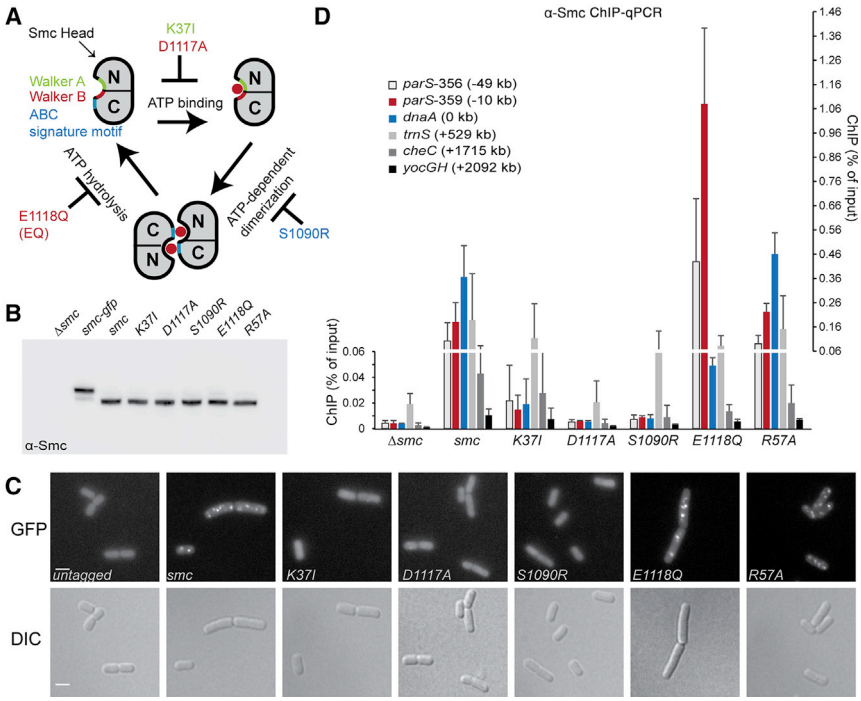

Figure 1. Smc ATPase Activity Determines the Chromosomal Distribution of Smc/ScpAB

(A) Schematic representation of the Smc ATPase cycle.

(B) Immunoblotting of ATPase mutant Smc proteins with α-Smc antiserum. Whole-cell extracts from strains BSG1002, BSG1007–BSG1008, BSG1067, BSG1045–BSG1047, and BSG1083. See also Figure S1B.

(C) Fluorescence images of cells harboring mGFP-tagged Smc alleles: BSG1002, BSG1067–BSG1068, BSG1855–BSG1857, and BSG1881. Scale bar, 2 μm. Differential interference contrast (DIC) (bottom) and GFP fluorescence images (top) are shown. Quantification of foci number per cell is given in Figure S1H.

(D) ChIP-qPCR analysis of cells from strains BSG1002, BSG1007–BSG1008, BSG1045–BSG1047, and BSG1083 using α-Smc antiserum. Error bars were calculated from two independent experiments as SD. Please note that values of ChIP enrichment below and above 0.06% are displayed on different scales given on the left and right side of the graph, respectively. The analysis of chromosomal loci harboring highly transcribed genes (such as the tRNA cluster *trnS*) generally produce ambiguous results with relatively high levels of ChIP signal in control samples (Δ*smc*). This seems to be a widely observed phenomenon in ChIP and it remains unclear whether the enrichment is physiologically relevant.

See also Figure S1.

chromosome. However, wild-type distribution of Smc on the bacterial chromosome—including its prominent localization to the replication origin—requires hydrolysis of ATP by Smc. Smc(R57A) showed a ChIP-qPCR pattern indistinguishable from wild-type Smc indicating that cellular ATP hydrolysis might be (if at all) only mildly affected by this amino-acid substitution in *B. subtilis*.

Smc/ScpAB Specifically Recognizes ParB/*parS* Nucleoprotein Complexes in Its Pre-hydrolysis State

To get a global view of the chromosomal distribution of Smc and Smc(EQ) proteins, we then analyzed ChIP input and eluate fractions by next-generation sequencing. Individual sequence reads were mapped to 1 kb sliding windows spaced at 100-bp intervals (Figure 2A) or to 5 kb bins (Figure 2C). In order to normalize for the copy number differences between origin-proximal and -distal loci caused by ongoing DNA replication, the ratio of the normalized number of reads in input and eluate fractions was calculated for each window. The resulting ChIP sequencing (ChIP-seq) profile for the Smc(EQ) sample showed striking peaks that are overlapping with several *parS* sites on the chromosome (Figure 2A). The profile of the wild-type sample is markedly different from the Smc(EQ) profile (Figure 2A) (Gruber and Errington, 2009). Its peaks at *parS* sites are less pronounced. Instead, other more prominent peaks are present at and near the replication origin (*oriC*) and generally more signal was detected all along the chromosome arms. Largely similar ChIP-seq results were obtained with an antiserum raised against the ScpB subunit (Figures S2 and 7A; discussed below), indicating that the observed enrichments are not caused by antibody artifacts and suggesting that substantial fractions of Smc and ScpB co-localize on the chromosome, presumably by forming Smc/ScpAB holo-complexes (Kleine Borgmann et al., 2013). ChIP-qPCR experiments using several primer pairs for chromosomal arm sites (Figure S2D) confirmed that Smc (but not Smc(EQ)) was significantly enriched at several positions on the two chromosome arms with levels of enrichment inversely correlating with distance from the replication origin. Together, these results confirm the specific localization of the Smc(EQ) protein to *parS* sites and strongly suggest that Smc head engagement is essential for Smc/ScpAB recruitment to the chromosome. However, a full cycle of ATP hydrolysis appears to be involved in the localization of Smc/ScpAB to other chromosomal sites—such as the replication origin and the chromosome arms (Figure 2A).

Furthermore, we found that the high levels of enrichment of Smc and Smc(EQ) at *parS-359* are fully dependent on the presence of ParB protein (Figure 3A). To compare the distribution of Smc and ParB proteins near *parS* sites, we next performed ChIP-seq analysis using an antiserum against the ParB protein. ChIP-seq peaks of ParB and Smc(EQ) (but not Smc) proteins at *parS* sites are very similar in terms of positioning and shape, strongly indicating that the two proteins are closely co-localized on chromosomal DNA (Figures 2A–2C and 2E).

In the absence of ScpA or ScpB, the Smc protein is non-functional and Smc-GFP fails to form foci in vivo (Lindow et al., 2002; Mascarenhas et al., 2002). We observed that the chromosomal

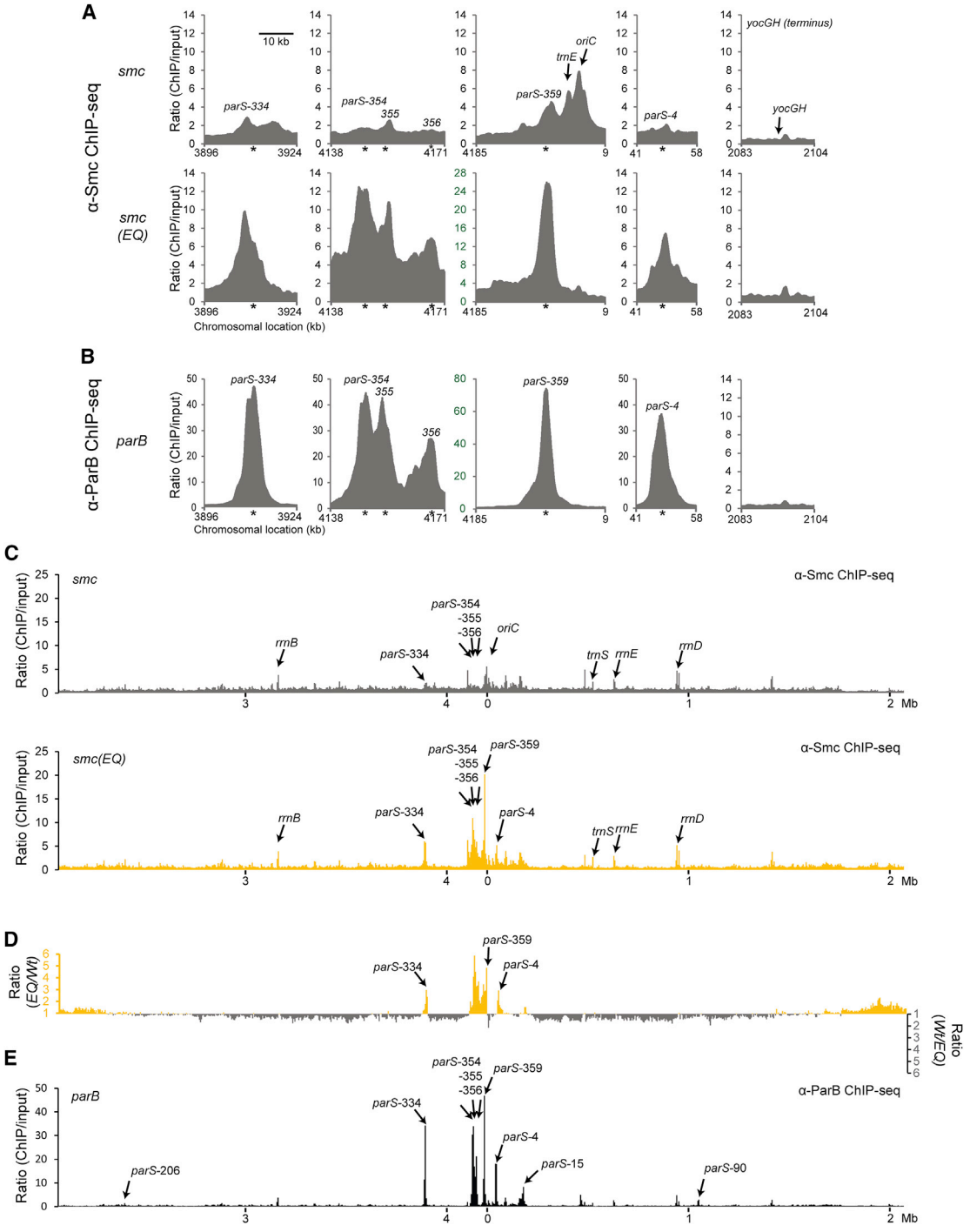

Figure 2. Hydrolysis Mutant but Not Wild-Type Smc Co-localizes with ParB/*parS*

(A) Close-up view of ChIP-seq profiles for wild-type Smc (BSG1002) (top panel) and Smc(EQ) (BSG1008) (bottom panel) generated using antiserum raised against the *Bs* Smc protein. Sequence reads were mapped to 1 kb windows spaced at 100-bp intervals and normalized for input DNA as follows. The number of reads for the ChIP sample in a given window was divided by the number of reads in the input sample for the same window (after normalizing the total number of reads). Raw input and ChIP data are shown in Figure S2. Axes labeled in green color highlights different scaling. Asterisks indicate the positions of *parS* sites.

(B) Close-up view of the ChIP-seq profile of ParB protein (from BSG1470 cells) generated using antiserum raised against purified *Bs*ParB-His6 protein. Data analysis and presentation as in (A).

(C) Whole-genome views of data presented in (A). Sequence reads were mapped to 5-kb windows spaced at 5-kb intervals across the genome and normalized for input DNA.

(legend continued on next page)

localization of wild-type Smc measured by ChIP-qPCR is strongly reduced when *scpA* or *scpB* is deleted (Figure 3B). Poor localization was also observed in Smc(EQ) cells in the absence of ScpA or ScpB. We thus conclude that ATP-dependent engagement of Smc heads as well as ScpA and ScpB proteins are crucial for efficient localization of Smc to ParB/*parS* on the chromosome. Apparently, a particular conformation of Smc/ScpAB recognizes ParB/*parS* nucleoprotein structures.

Dimerization at the Smc Hinge Controls Chromosomal Association of Smc/ScpAB

Next, we investigated the role of the Smc hinge domain in the localization of Smc/ScpAB to the bacterial chromosome. We made use of a previously characterized mutation of four highly conserved glycine residues to alanine at the *Bs* Smc hinge-hinge interface (designated as "mH" for mutant hinge) to block formation of stable dimers at the Smc hinge domain (Hirano and Hirano, 2002) (Figures S3C and S3D). The ChIP-qPCR enrichment of Smc(mH) was clearly reduced at *parS-359* as well as *dnaA* (Figure 3C). Dimerization of Smc at the hinge thus seems to be important for localization of wild-type Smc/ScpAB to the chromosome. This is consistent with the notion that Smc/ScpAB associates with the chromosome by entrapping the chromosomal DNA double helix within its SMC/kleisin ring (Wilhelm et al., 2015). In stark contrast, however, the enrichment of Smc(mH-EQ) protein at *parS-359* (but not at *dnaA*) was strongly enhanced (~4-fold) compared to Smc(EQ) (Figure 3C). Thus, hinge dimerization has strikingly antagonistic effects on the association of Smc and Smc(EQ) with the chromosome. Remarkably, ScpA and ScpB are dispensable for targeting of Smc(mH-EQ) to the chromosome (Figures 3C and S3H), while they are essential for wild-type Smc and Smc(EQ) to localize to the chromosome (Figure 3B). A plausible explanation for these striking observations is that the ScpAB sub-complex counteracts an inhibitory function of hinge dimerization on chromosomal targeting of Smc.

To ensure that these surprising findings are not caused by artifacts in the chromatin immunoprecipitation procedure, we have analyzed a set of Smc mutants by live-cell imaging of fluorescently labeled Smc proteins (Figure 3D). As predicted from the ChIP experiments, Smc(EQ)-GFP failed to form chromosomal foci when *scpA* is deleted, while Smc(mH-EQ)-GFP produced bright foci irrespective of the presence and absence of *scpA*. Together, these findings corroborate the view that Smc complexes associate with the bacterial chromosome in two fundamentally distinct manners, which are defined by the state of the Smc ATPase.

Smc Hinge Dimerization Inhibits Smc Head Engagement

How might the ScpAB sub-complex and dimerization at the Smc hinge control targeting of Smc to chromosomal *parS* sites in antagonistic ways? Conceivably, ScpAB and the Smc hinge might positively and negatively influence the engagement of Smc head domains, respectively, and thereby regulate the recruitment of Smc/ScpAB to *parS*. If so, then the levels of head engagement should correlate with the efficiency of chromosomal targeting. To address this, we made use of the efficient chemical cross-linking of closely juxtaposed pairs of cysteines by a thiol-specific bis-maleimide compound (BMOE) in *B. subtilis* (Bürmann et al., 2013; Soh et al., 2015). Based on the crystal structure of the *Pyrococcus furiosus* Smc(EQ) head dimer in the presence of ATP (Lammens et al., 2004), we engineered a cysteine residue into the bottom surface of the *Bs* Smc head (K1151C), so that it is located in close proximity to its pair mate at the 2-fold symmetry axis of the dimer (Figure 4A). In order to be able to precisely quantitate the levels of cross-linking, we fused the cysteine bearing *smc* gene at its C terminus with a HaloTag thus allowing in-gel fluorescence detection of Smc. In addition, the four endogenous cysteines in Smc were replaced by serine residues to reduce the propensity for any off-target cross-linking (Hirano and Hirano, 2006). The corresponding *smc* allele supports growth on nutrient rich medium, implying that it is functional (Figure S4A). Cross-linking of K1151C in otherwise wild-type Smc was barely detectable (<4%), while the ATP hydrolysis mutant Smc produced a low but substantial fraction (~14%) of cross-linked Smc dimers (Figure 4B). Intriguingly, K1151C cross-linking was undetectable in Smc(mH) but very pronounced in Smc(mH-EQ). The latter is cross-linked with an efficiency comparable to those previously observed for other Smc-Smc, Smc-ScpA, and DnaN-DnaN interfaces, which strongly suggests that the K1151C residue is a good reporter for head-head association (Bürmann et al., 2013; Soh et al., 2015; Wilhelm et al., 2015). The low levels of cross-linking observed with wild-type Smc and Smc(EQ) are therefore in most likelihood due to poor efficiency of head engagement. Deletion of *scpA* or *scpB* decreased the cross-linking of K1151C in Smc and Smc(EQ) protein even further (Figures 4B and S4B) being consistent with the notion that ScpAB might stimulate the targeting of Smc(EQ) to the chromosome (Figures 3B and S3H)—at least partly—by promoting head engagement (Bürmann et al., 2013; Kamada et al., 2013).

Smc head engagement must be a transient or rare phenomenon since it is barely detectable by cross-linking in wild-type Smc/ScpAB (Figure 4B). The maintenance of its association with the chromosome is thus very likely independent from continuous engagement of head domains. Smc head engagement, however, must be crucial during the establishment of chromosome association, because mutants defective in head engagement are unable to bind to the chromosome altogether. A stable association with the chromosome is likely created via the entrapment of chromosomal DNA within the Smc/ScpAB ring, a process that we have recently shown to be dependent on ATP hydrolysis (Wilhelm et al., 2015). We thus propose that Smc/ScpAB displays two distinct modes of binding to the

(D) To highlight differences between the distribution of wild-type Smc and Smc(EQ) the normalized ratios for Smc(EQ) in a given window was divided by the equivalent ratio for Smc(wt). Numbers above one are shown in yellow colors (axis on the left side). For numbers below one, the inverse ratio was calculated and displayed in gray colors (axis on the right side).
(E) Whole-genome view of the ParB ChIP-seq data presented in (B). Data analysis as in (C).
See also Figure S2.

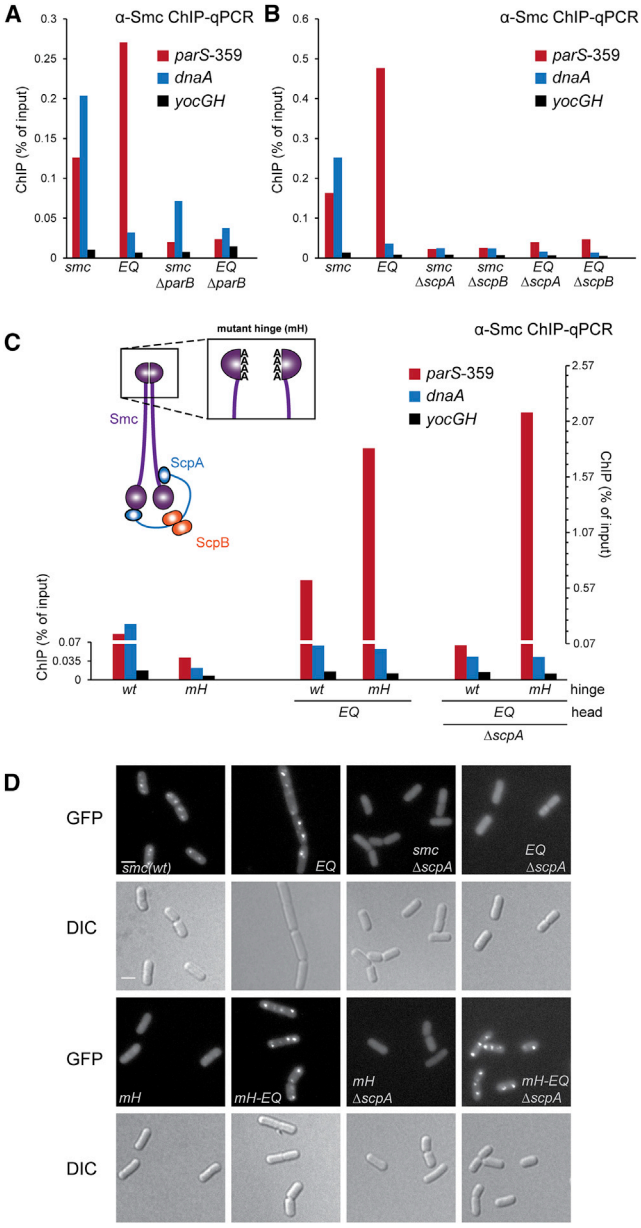

Figure 3. Dimerization at the Smc Hinge Hinders Chromosomal Association of Smc/ScpAB

(A) ChIP-qPCR was performed on exponentially growing cells of strains BSG1051–BSG1052, BSG1406, and BSG1387 using α-Smc antiserum. Quantification of input and eluate material was done by qPCR using primer pairs specific for the indicated loci.

(B) As in (A) using strains BSG1889–BSG1894.

(C) The scheme indicates the disruptive effect of mutations in the Smc hinge domain on dimerization. ChIP-qPCR was performed with α-Smc antiserum on strains BSG1620–BSG1621, BSG1624, BSG1890, and BSG1892–BSG1893.

(D) Fluorescence imaging of Smc-mGFP fusion proteins in cells of strains BSG1067–BSG1068, BSG1378, BSG1413, BSG1662, BSG1677, and BSG1798–BSG1799. Scale bar, 2 μm. Quantification of foci number per cell is given in Figure S4C. Same experiments as in Figure 1C.

See also Figure S3.

chromosome. The first one, designated as pre-hydrolysis mode, occurring mostly or exclusively at *parS* sites presumably via a physical interaction with the chromosome, has a strict requirement for Smc head engagement. The second one, generated by transient head engagement and subsequent ATP hydrolysis, designated as post-hydrolysis mode, features a much more dispersed distribution on the bacterial chromosome and likely involves the entrapment of one or more DNA double helices within the Smc/ScpAB ring.

Rod-Shaped Smc Dimers Poorly Target ParB/*parS*

The levels of head engagement in Smc, Smc(EQ), and Smc(mH-EQ) correlate well with their efficiency of targeting to *parS* on the chromosome (Figures 3C and 4B). However, when *scpA* is deleted, both Smc(EQ) and Smc(mH-EQ) display similarly low levels of head cross-linking, whereas Smc(mH-EQ) but not Smc(EQ) exhibits strong enrichment at *parS* on the chromosome (Figures 3C and 4B). We conclude that hinge dimerization must have additional effects on Smc(EQ), through which it restricts chromosomal targeting, and Smc head engagement—albeit being essential—is not sufficient for targeting of Smc/ScpAB to *parS* sites.

Smc dimers form straight rods via the close juxtapositioning of the Smc coiled coils (Soh et al., 2015). Upon Smc head engagement and DNA binding, however, they have been proposed to undergo an extensive conformational change to a more open, possibly ring-like configuration in vitro (Soh et al., 2015). Conceivably, this structural transition might also regulate the binding of Smc/ScpAB to ParB/*parS*. If this were the case, then any Smc mutant that efficiently targets to *parS* might harbor unstable Smc rods. To investigate this, we employed in vivo cross-linking of a cysteine residue (A715C) located at the hinge-proximal interface between the two Smc coiled coils as an indicator for the formation of Smc rods (Figure 4C) (Soh et al., 2015). As reported previously, ~35% of wild-type Smc(A715C) proteins were cross-linked into covalent dimers by BMOE (Figure 4C). The mutant hinge strongly decreased the fraction of Smc dimers displaying coiled coil rods, irrespective of the presence or absence of ScpA protein (Figure 4C). Similarly, the E1118Q mutation lead to a significant reduction in the fraction of Smc dimers with rod-shaped coiled coils providing direct evidence that the ATPase cycle affects the architecture of the Smc coiled coils near the Smc hinge in vivo. Crucially, the partial dissolution of Smc(EQ) rods was lost when the *scpA* gene was deleted, whereas the more pronounced opening of the coiled coils in Smc(mH, EQ) was unaffected by *ΔscpA*. The ScpA subunit thus facilitates the opening of the Smc rod (Figures 4B and 4C). Altogether, these data strongly support the notion that dimerization at the Smc hinge promotes Smc rod formation, which in turn opposes head engagement. ScpA is required to antagonize rod-stabilization exerted by the Smc hinge and consistent with this notion it becomes dispensable for rod opening (and chromosomal targeting) in the absence of a functional hinge. Hence, a combination of two interrelated structural features seems to be responsible for the targeting of Smc/ScpAB to *parS* sites on the chromosome: (1) engagement of Smc head domains, and (2) dissolution of the Smc rod. Both features appear to be rare

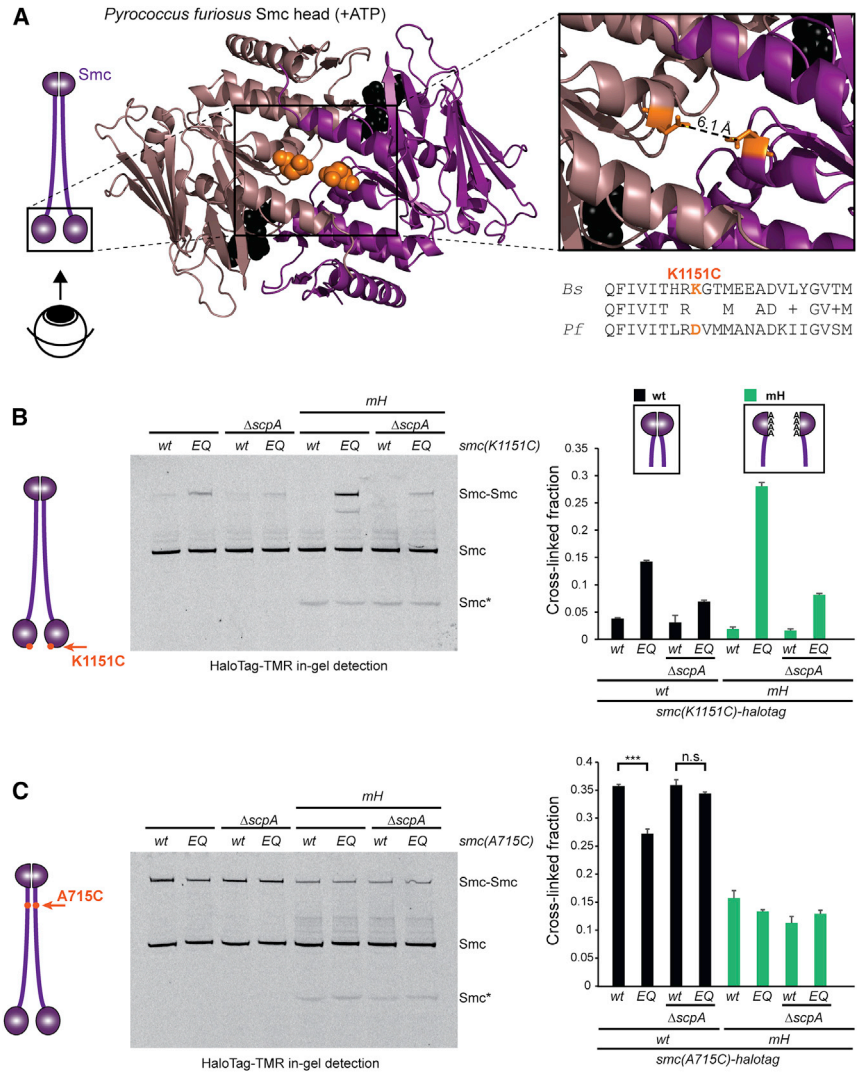

Figure 4. Hinge Dimerization and Head Engagement Control the Conformation of Smc/ScpAB

(A) Structure of ATP engaged *Pf* Smc head domains (PDB: 1XEX) in brown and pink colors, respectively, (bottom view). Residue D1131 is indicated in ball representation in orange colors (middle panel). The distance between the carboxyl carbon atom in the side chains of the D1131 symmetry mates is estimated to be ~6 Å (right panel). A sequence alignment between *Pf*Smc and *Bs*Smc shows that K1151 in *Bs*Smc corresponds to D1131 in *Pf*Smc.

(B) In vivo BMOE crosslinking of Smc(K1151C)-HaloTag in cells of strains BSG1488, BSG1509, BSG1512, BSG1547, BSG1597–BSG1598, BSG1791, and BSG1800. Four endogenous cysteine residues were replaced by serines. Crosslinked Smc-Halotag species were detected by in-gel fluorescence of the HaloTag-TMR substrate (left panel). Smc* indicates a degradation product of Smc(mH). The graph (right panel) shows mean values and SDs from three replicates.

(C) Same as in (B) using A715C as sensor cysteine for formation of Smc rods by the hinge proximal Smc coiled coil. In vivo crosslinking of Smc (A715C) with bismaleimidoethane (BMOE) in strains BSG1921–BSG1924, BSG1949–BSG1951, and BSG2036. T test statistics: ***$p \leq 0.001$; not significant (n.s.), $p > 0.05$.

See also Figure S4.

or short-lived in wild-type Smc/ScpAB, presumably due to the inhibition by the hinge and the destabilizing action of the Smc ATPase. Nevertheless, a large fraction of cellular Smc/ScpAB must at least transiently adopt this conformation in order to localize to the replication origin region and to be able to form Smc-GFP foci in vivo (Figure 1) (Gruber and Errington, 2009; Sullivan et al., 2009).

Concomitantly, our A715C cross-linking experiments indicate that Smc coiled coils can be juxtaposed in a sizeable fraction of proteins even when dimerization at the Smc hinge is impaired, the ScpA bridge absent and Smc heads almost completely disengaged (Figure 4B). Thus, the association between Smc coiled coils contributes considerably to Smc dimerization.

The Smc Hinge Domain Is Dispensable for Targeting to *parS* DNA

A DNA binding site has previously been mapped to the bottom surface of the *Bs* Smc hinge dimer (Hirano and Hirano, 2006; Soh et al., 2015). DNA binding at the coils/hinge junction appears to be sterically blocked by the juxtapositioning of the Smc coiled coils and promoted by ATP-dependent dissolution of the Smc rod (Soh et al., 2015). The same mechanism could be responsible for the targeting of Smc/ScpAB to *parS* sites on the chromosome. If ParB/*parS*—like naked DNA—were to bind to the bottom of the Smc hinge dimer, then the presence of the hinge domain would be crucial for localization of Smc(EQ) to the chromosome. To test this, we constructed an Smc fragment lacking the entire hinge domain ("ΔH" for hinge deletion) by connecting the end of Smc's N-terminal coiled coil helix (amino acids 1–499) to the start of the C-terminal coiled coil helix (aa 674–1186) using a flexible linker peptide (-GGGSGGGSGGG-). The Smc(ΔH) construct was fused to a TAP tag at its C terminus and integrated at the endogenous *smc* locus. Smc(ΔH) was expressed at normal levels in *B. subtilis* but failed to localize to the chromosome as judged by α-TAP ChIP (Figures 5A and S5A). However, a Smc(ΔH) variant harboring the E1118Q mutation displayed robust localization to *parS*-359 in the presence and absence of the ScpA subunit (Figure 5A). Overall, strains harboring either a mutant Smc hinge domain or a complete deletion of the Smc hinge produced very similar results, clearly demonstrating that the Smc hinge is dispensable for the targeting of Smc(EQ) to *parS* (Figure 5A) and confirming that the hinge domain regulates chromosomal targeting indirectly—likely by affecting other parts of the Smc/ScpAB complex.

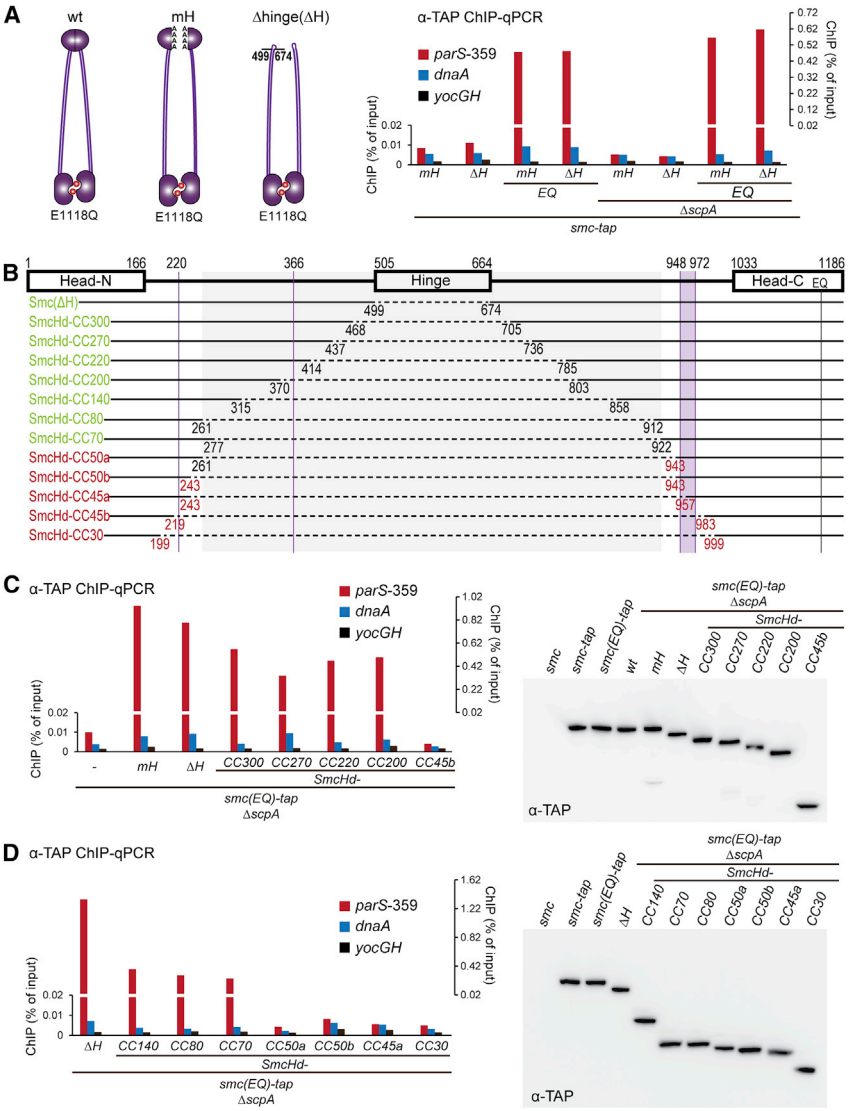

Figure 5. A Large Central Part of Smc Is Dispensable for Targeting to *parS*

(A) ChIP-qPCR was performed with TAP-tagged alleles of Smc using IgG-coupled magnetic beads for immunoprecipitation. Strains: BSG1671–BSG1672, BSG1689, BSG1691, BSG1779–BSG1780, and BSG1895–BSG1896. The schemes on top represent modifications to the Smc hinge in Smc(mH) (left) and Smc(ΔH) (right).

(B) Schematic overview of the series of internal Smc truncation constructs. Solid and dashed horizontal lines denote the presence and absence of Smc sequences in a given truncation construct. A gray box demarcates the central portion of the Smc protein, which is dispensable for targeting to *parS-359*. N-terminal and C-terminal Smc sequences are fused via a short peptide linker (-GGGSGGGSGGG-). The name of a given truncation construct indicates the predicted length of its Smc coiled coil. Labels in green and red colors indicate efficient and inefficient targeting to *parS*. All proteins are tagged with a TAP tag at their C terminus. Purple vertical lines and boxes indicate disruptions in the Smc coiled coil (Waldman et al., 2015).

(C) ChIP-qPCR against the TAP tag of strains BSG1520, BSG1689, BSG1779, BSG1825, BSG1871–BSG1872, and BSG1874–BSG1875 (left panel). Immunoblot against the TAP tag with strains BSG1002, BSG1016, BSG1475, BSG1520, BSG1689, BSG1779, BSG1825, BSG1871–BSG1872, and BSG1874–BSG1875 (right panel).

(D) Same as in (C) with another set of Smc truncation constructs. ChIP-qPCR with strains BSG1779, BSG1824, BSG1826–BSG1830 and BSG1873 (left panel). Anti-TAP immunoblot with strains BSG1002, BSG1016, BSG1475, BSG1779, BSG1824, BSG1826–BSG1830, and BSG1873 (right panel). See also Figure S5.

A Mini-Smc Localizes to *parS* Sites on the Chromosome

The above results demonstrate that neither the Smc hinge nor the ScpA and ScpB subunits are strictly required for the localization of Smc(EQ) to *parS* sites. In order to fine map potential binding sites for ParB/*parS* on the Smc(EQ) protein, we removed increasingly larger segments of the central part of a Smc(EQ)-TAP allele by fusing selected N- and C-terminal Smc sequences using a short linker peptide (Figure 5B). Twelve such Smc fragments (designated as SmcHd-CC330 to SmcHd-CC30) were integrated into the endogenous *smc* locus by allelic replacement in a Δ*scpA* strain. All these truncated Smc(EQ) proteins were expressed at normal levels in *B. subtilis* as judged by immunoblotting against the TAP tag (Figures 5C and 5D). Intriguingly, the seven larger fragments (SmcHd-CC330–SmcHd-CC70) yielded strong and specific enrichment at the *parS-359* locus similar to the Smc(mH-EQ) and Smc(ΔH-EQ) proteins. In contrast, the five shorter constructs (SmcHd-CC50a– SmcHd-CC30) lacked any specificity for *parS-359* and instead displayed background levels of enrichment at all tested loci (Figures 5C and 5D). These results demonstrate that a large, central portion of Smc—comprising its hinge domain and approximately two-thirds of the hinge proximal coiled coil—is dispensable for the specific recognition of ParB/*parS*. A region located within the head proximal part of the Smc coiled coil, however, appears to be critical for *parS* targeting because even small truncations in this region totally abolish localization to *parS*. An Smc moiety critical for localization to *parS* thus appears to be located around hundred amino acid residues away from the Smc head domain on the Smc coiled coil. Mapping of the coiled coil register demonstrates that this head-proximal third of the Smc coiled coil includes a region in which the heptate register is interrupted in the N-terminal coiled coil helix and a 24 amino acid long peptide is inserted into the C-terminal α-helix (Figure S5D), (Waldman et al., 2015). Possibly, these extra sequences protrude from the Smc coiled coil and might be involved in the interaction with ParB protein and/or *parS* DNA. In the rod configuration, however, the protrusions might be sterically obstructed or otherwise masked.

Smc/ScpAB Relocates from *parS* Loading Sites to Distant Parts of the Chromosome in an ATP Hydrolysis-Dependent Manner

Smc/ScpAB exhibits very high specificity for *parS* sites on the bacterial chromosome when it is locked in its pre-hydrolysis conformation (Figures 1D and 2D). Nonetheless, only a small proportion of wild-type Smc/ScpAB actually localizes to *parS* sites in *B. subtilis* as judged from anti-ScpB and anti-Smc ChIP-seq profiles (Figures 2A and 6A). In fact, Smc/ScpAB rather displays a very broad distribution over the bacterial chromosome with a moderate peak at the replication origin and shallow gradients toward the replication terminus along both arms of the chromosome (Figures 6A and S2C) (Gruber and Errington, 2009). Formation of this long range gradient is completely abolished in the absence of ParB protein (Figure 6A). This raises the intriguing question of how a highly-localized pool of ParB protein might establish a very wide gradient of Smc/ScpAB on the chromosome. Conceivably, Smc/ScpAB might first load onto the chromosome at a *parS* site and then redistribute into neighboring and more distant regions of the chromosome. To test this, we modified the pattern of chromosomal recruitment of Smc/ScpAB by inserting a single additional *parS* site into the *B. subtilis* chromosome and observed changes in the chromosomal distribution of wild-type Smc/ScpAB. We inserted a 75-bp fragment of the *parB* gene including the *parS*-359 site or its non-functional variant, *mparS*, into the non-essential *amyE* gene located ~330 kb away from the replication origin on the right arm of the chromosome. The presence of the ectopic *parS* site at *amyE*, designated as *parS-amyE*, had no discernible effects on the growth of *B. subtilis*. We then tested whether the artificial *parS-amyE* locus serves as chromosomal landing site for Smc/ScpAB using ScpB ChIP-seq experiments in strains harboring the *smc(EQ)* gene (Figure S6). Efficient targeting of Smc(EQ) to *parS-amyE* suggests that also a significant fraction of wild-type Smc/ScpAB is loaded onto the chromosome at the synthetic *parS-amyE* locus (Figure S6). The pattern of wild-type Smc/ScpAB localization measured by ScpB ChIP-seq was superficially similar in cells harboring the ectoptic *parS* or *mparS* site (Figure 6B). However, the levels of ScpB enrichment were moderately—but consistently—higher for example in a region between the replication origin and the *amyE* locus when the additional *parS* site was present. In order to get a global and more quantitative picture of the differences between the two ChIP samples, we calculated enrichment ratios for each window along the chromosome (Figure 6B). Strikingly, the differences between the two samples followed a clear pattern with opposite trends on the two arms of the chromosome. Almost all loci on the right arm of the chromosome, which includes the ectopic *parS* site, were more highly enriched (on average by ~20%) in the *parS-amyE* sample, whereas DNA from the left arm of the chromosome was generally more enriched (~20%) in the *mparS* sample. Clearly, the addition of a single *parS* site at a defined position on the chromosome affects Smc distribution in a chromosome arm-specific manner. What might be the underlying molecular mechanism? Smc/ScpAB could relocate from *parS* by three-dimensional (3D) diffusion within a chromosomal domain or by one-dimensional (1D) translocation along the DNA backbone. 3D diffusion seems a highly unlikely explanation for intra-arm-specific relocation because loci on opposite chromosome arms are thought to be in close proximity in *B. subtilis* (Le et al., 2013; Marbouty et al., 2014, 2015; Umbarger et al., 2011; Wang et al., 2015). Our data is much more consistent with 1D translocation of Smc/ScpAB along a DNA double helix within a chromosome arm. According to this hypothesis, loading of Smc/ScpAB at the ectopic *parS* site might titrate condensin away from endogenous *parS* sites and thereby reduce loading on one arm of the chromosome, while increasing the fraction loaded onto the other. Curiously, the re-distribution of Smc complexes loaded onto the chromosome at the ectopic *parS* site appears to occur differently toward the replication origin and the terminus. In *B. subtilis*, most genes are co-oriented with respect to DNA replication. Thus, the apparent difference in relocation toward and away from the replication origin might be due to head-on encounters with transcription or replication complexes (Wang et al., 2015). Overall, these experiments provide evidence that Smc/ScpAB is able to translocate along a DNA double helix over large distances on the bacterial chromosome after its release from *parS* sites.

DISCUSSION

The mechanistic bases for SMC's dynamic association with chromosomes are in many ways mysterious. Here, we reveal that the Smc ATPase cycle defines two different configurations of Smc/ScpAB, which distinctly interact with the bacterial chromosome. The pre-ATP hydrolysis state displays high specificity for *parS* proximal DNA, whereas the specificity for *parS* is lost upon ATP hydrolysis leading to the redistribution of Smc/ScpAB within the chromosome.

Pre-ATP Hydrolysis Smc/ScpAB: A Tightly Regulated Configuration for ParB/*parS* Targeting

Our findings define the ATP engaged form of SmcHd(EQ)-CC80 as minimal structure for the specific recognition of Smc/ScpAB's chromosomal target (Figure 5). They highlight the importance of a head proximal segment of the Smc coiled coil in *parS*-DNA targeting and raise intriguing questions. How is binding of Smc/ScpAB to ParB/*parS*-DNA enabled by Smc head engagement? And conversely, how is physical association with the chromosome blocked when Smc heads are disengaged? Based on the strict dependence of *parS* targeting on Smc head engagement and its inverse correlation with Smc rod formation, we propose that a putative interface for ParB/*parS* on the head-proximal Smc coiled coil is concealed or distorted within the Smc rod. Smc head engagement might simply trigger the opening of the Smc rod and thereby unmask an interfaces for binding to ParB/*parS*. However, dimerization defective Smc proteins only very poorly localize to *parS* sites, despite featuring mostly "disengaged" Smc coiled coils (Figures 4 and 5). Conceivably, the interaction via a single interface on monomeric Smc is too transient for significant levels of targeting to *parS*. If so, then Smc head engagement might arrange the two interfaces on a given Smc dimer in a way that allows them to co-operatively and thus more stably bind a ParB protein/*parS* DNA complex. In this regard, it is tempting to speculate that DNA passes between the Smc coiled coils, because in this instance the 2-fold

Please cite this article in press as: Minnen et al., Control of Smc Coiled Coil Architecture by the ATPase Heads Facilitates Targeting to Chromosomal ParB/*parS* and Release onto Flanking DNA, Cell Reports (2016), http://dx.doi.org/10.1016/j.celrep.2016.01.066

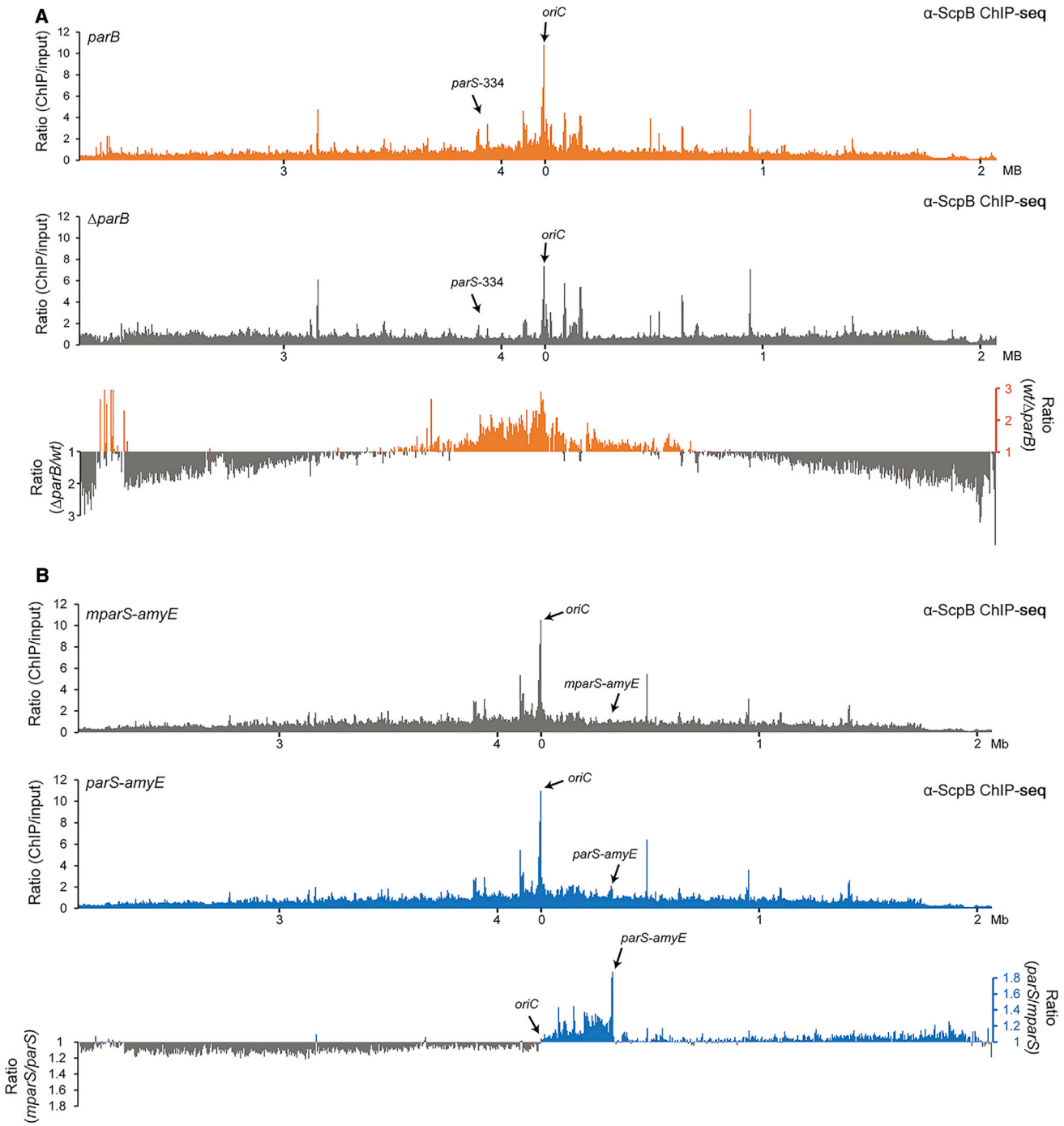

Figure 6. Smc/ScpAB Relocates from *parS* Loading Sites to Distant Parts of the Chromosome upon ATP Hydrolysis

(A) ChIP-seq using α-ScpB antiserum on strains BSG1002 (*parB*) (top panel) and BSG1052 (Δ*parB*) (middle panel). Reads were mapped to 5-kb bins. Signals for IP samples were divided by the signals of the normalized input. Ratios were calculated by dividing the values obtained for the wild-type strain by the numbers of the Δ*parB* strain (bottom panel). All values above one are shown in orange colors. For all other windows the inverse ratio was calculated and displayed in gray colors.

(B) ChIP-seq using α-ScpB antiserum on strains BSG1470 (*mparS-amyE*) (top panel) and BSG1469 (*parS-amyE*) (middle panel). Reads were mapped to 5-kb bins. Signals for IP samples were divided by the signals of the normalized input. Ratios were calculated by dividing the values of the *parS-amyE* strain by the *mparS-amyE* strain (bottom panel). A number above one indicates more reads in the *parS-amyE* sample (shown in the blue colors), for all other windows, the inverse ratios were calculated and displayed in gray colors.

See also Figure S6.

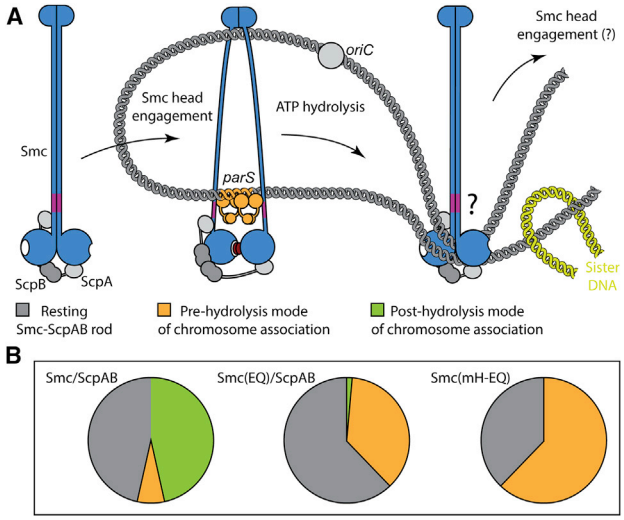

Figure 7. Model for the Recruitment of Smc/ScpAB to and Release from *parS* Sites

(A) Model for the targeting to and release from ParB/*parS* by holo-Smc/ScpAB. Most Smc/ScpAB exists as a rod-shaped structure, which is unable to bind to DNA via its hinge or to ParB/*parS* via the coiled coils. Dissolution of the Smc rod and engagement of Smc head domains are prerequisites for the targeting of Smc/ScpAB to *parS*. Upon ATP hydrolysis, the ring-like structure might revert to the rod conformation and is released from *parS* DNA. Sister DNA segments (in green colors) might be excluded from the Smc rod due to steric restrictions. Repetitive rod-ring-rod transitions might drive DNA loop extrusion.

(B) Pie charts displaying rough estimates for the relative occupancy of the different states illustrated in (A) based on Smc head cross-linking efficiency (Figure 4B). Please note that the fraction of wild-type Smc complexes on and off the chromosome (depicted as green and gray pies in the left chart) is unknown. A tiny fraction of chromosomally loaded Smc(EQ)/ScpAB has been detected (Wilhelm et al., 2015).

symmetry axis in the Smc dimer is matched to the one in ParB dimers. Binding of Smc to ParB/*parS*-DNA would therefore be restricted to the rare occasions when Smc head domains engage with one another to dissolve the Smc rod.

Although we have not been able to directly detect the recruitment of wild-type Smc to *parS* sites, at least three observations strongly suggest that wild-type Smc (like Smc(EQ)) is targeted to *parS* on the chromosome. First of all, the formation of chromosomal foci by wild-type Smc/ScpAB as well as its localization to the replication origin depend on ParB protein and *parS* sites (Gruber and Errington, 2009; Sullivan et al., 2009). Second, the efficiency of DNA entrapment by Smc/ScpAB is strongly decreased by the absence of ParB, indicating that most Smc/ScpAB is loaded onto the chromosome at *parS* sites (Wilhelm et al., 2015). Third, the chromosomal distribution of Smc is changed by an additional *parS* site. We propose that transient head engagement in Smc/ScpAB governs its brief encounters with chromosomal *parS* sites. It is important to note that the Smc(EQ) protein might display residual levels of ATP hydrolysis activity (Hirano and Hirano, 2004). It is thus conceivable that some observations made with Smc(EQ) such as its dependence on ScpAB during head engagement and *parS* localization and the inhibition by hinge dimerization might be specific to this partially defective ATP hydrolysis mutant. Furthermore, it is possible that the association of Smc(mH-EQ) (and Smc(EQ)/ScpAB) with ParB/parS might be structurally somewhat different from wild-type Smc/ScpAB.

Smc/ScpAB Relocation on the Bacterial Chromosome

The chromosomal distribution of Smc/ScpAB displays a single, broad peak centered on the replication origin and extending all the way to the replication terminus region (Figure 6A). Formation of such molecular gradients can be explained by a localized source of molecules and their random/diffusional or directed motion away from the source. Loading at *parS* establishes a tightly localized source of chromosomal Smc/ScpAB. Here, we present evidence for the subsequent relocation of Smc/ScpAB from its loading sites into flanking DNA. Our findings are consistent with the idea that Smc/ScpAB is able to translocate on the bacterial chromosome over hundreds of kilobases. Interestingly, cohesin has also been suggested to move away from its loading sites upon ATP hydrolysis possibly over several tens of kilobases (Hinshaw et al., 2015; Hu et al., 2011). What might be the purpose of such a striking and apparently conserved propensity for chromosomal relocation and what could be the molecular driving force?

The association of SMC complexes with chromosomes by DNA entrapment provides an obvious basis for a DNA sliding mechanism. Sliding of Smc/ScpAB rings along a single DNA molecule could help to identify and eliminate tangles within chromosomal DNA or between sister DNA molecules and thus promote chromosome segregation. However, this simple mechanism by itself fails to explain how Smc/ScpAB could organize the chromosome. Conceivably, Smc/ScpAB (like cohesin in eukaryotes) acts as a DNA clamp by capturing two or more DNA double helices within a single Smc/ScpAB ring or through the association of two or more Smc/ScpAB rings each entrapping a single DNA double helix. Taking into account the proposed DNA relocation activity, DNA loops could be formed by Smc/ScpAB and continuously expanded by the translocation of DNA through Smc/ScpAB rings. Extrusion of DNA loops—created at a *parS* site—explains how the left arm of the chromosome might be brought together with its right counterpart to establish the longitudinal organization of the chromosome observed in *Caulobacter crescentus* and *B. subtilis* (Le et al., 2013; Marbouty et al., 2014, 2015; Umbarger et al., 2011; Wang et al., 2015). Loop extrusion by SMC complexes also provides a simple solution for the formation of linearly condensed rod-shaped chromosomes during mitosis (Alipour and Marko, 2012; Bürmann and Gruber, 2015; Nasmyth, 2001). However, the driving force for any proposed relocation and loop extrusion mechanisms remains enigmatic. Smc/ScpAB appears to be able to translocate on the bacterial chromosome against the flow of replication forks and active transcription units, making a role of RNA polymerase and replication fork proteins in translocation unlikely (Figure 6) (Wang et al., 2015). Smc itself is an enzyme that could harbor energy from the hydrolysis of ATP to perform work. In principle, it could act as a motor protein for example by using its head engagement/disengagement cycle to progressively move DNA through its ring in a directional manner (Figure 7). For example, repetitive transitions between Smc rod

Please cite this article in press as: Minnen et al., Control of Smc Coiled Coil Architecture by the ATPase Heads Facilitates Targeting to Chromosomal ParB/*parS* and Release onto Flanking DNA, Cell Reports (2016), http://dx.doi.org/10.1016/j.celrep.2016.01.066

and Smc ring states might allow continuous expansion of loops of chromosomal DNA formed at *parS* (Figure 7) (Alipour and Marko, 2012; Nasmyth, 2001). Our data indeed suggest that ATP hydrolysis by Smc/ScpAB is involved in its chromosomal redistribution after loading. However, it remains to be determined whether continuous ATP hydrolysis by Smc is needed for relocation to distant positions on the chromosome or whether a single round of ATP hydrolysis is sufficient to trigger the relocation process.

The Mechanics of Smc Rod Making and Rod Breaking

We discovered an unexpected antagonistic functional relationship between the two globular domains located at distal ends of the long Smc coiled coil: dimerization at the Smc hinge has a clear inhibitory activity on the engagement of Smc head domains. Conversely, head engagement reduces the level of Smc coiled coil alignment. How might this long-distance communication happen mechanistically? We propose that the Smc coiled coil acts as rather stiff rod, which positions the Smc head in a way that is incompatible with ATP-dependent head engagement when the two Smc coiled coils are being aligned side-by-side. Dimerization of Smc hinge domains ("rod maker") promotes Smc rod formation presumably by simply bringing the ends of two Smc coiled coils in close proximity in a way that allows them to zip up. Head engagement with the help of ScpAB ("rod breakers"), however, positions the two other ends of the Smc coiled coils at a distance to each other, thus favoring the unzipping of the Smc rod. In analogy, to the role of NBDs in ABC transporters, engagement and disengagement of Smc head domains might transform the Smc coiled coil between a rod-like state and a more open ring-like state. Only the open state appears to be able to contact DNA and the ParB/*parS* substrates via two separate interfaces located at the Smc hinge and within the head proximal coiled coil, respectively. Substrate binding is then likely triggering ATP hydrolysis, thereby driven head disengagement and rod re-formation, which in turn releases DNA and ParB/*parS* from its binding sites (Figure 7). We propose that transitions between open and closed states are central aspects of SMC biochemistry – conceivably regulating substrate binding to many or all SMC/kleisin complexes.

EXPERIMENTAL PROCEDURES

Strain Construction

Genetic modifications were introduced via double cross-over recombination into the genome of *B. subtilis 1A700*. Cells were made competent and grown on SMG or NA medium supplied with antibiotics as previously described (Bürmann et al., 2013). Relevant genotypes are given in Table S1.

ChIP-qPCR

ChIP-qPCR experiments were essentially performed as previously described (Gruber and Errington, 2009). Detailed information is available in the Supplemental Information.

ChIP-Seq

ChIP samples were prepared as described above with the exception that several immunoprecipitate (IP) samples were loaded onto the same PCR purification column to obtain sufficient DNA material. DNA (1–5 ng) was analyzed by Illumina sequencing at the Max Planck Genome Centre in Cologne. Briefly, DNA was fragmented by sonication (Covaris S2) to fragment sizes ranging from 220–280 bp with a main peak of ~250 bp. DNA libraries were prepared using the Ovation Ultralow Library System (NuGEN) kit (version V1) including 15 cycles of PCR amplification. Five to ten million sequence reads were obtained on a HiSeq2500 (Illumina) with 100-bp read length. The obtained reads were mapped to the genome with Bowtie (http://GalaxyProject.org) using default settings and randomly assigning sequencing reads from repetitive DNA elements to a single location. Subsequent data analysis was performed using Seqmonk (http://www.bioinformatics.babraham.ac.uk/projects/seqmonk/) and Microsoft Excel.

BMOE Cross-Linking

In vivo cross-linking of cysteine-modified Smc protein was performed as described previously (Soh et al., 2015).

Microscopy

Overnight cultures in SMG medium were diluted to an OD_{600} of 0.005 and grown to OD_{600} 0.02–0.03 in SMG medium. Cells were mounted on agarose pads and visualized on an Applied Precision DeltaVision RT system equipped with an Olympus IX-71 inverted base microscope, an Olympus UPlanApo 100 ×/NA1.35 oil immersion objective and a Photometrics CoolSNAP HQ 12 bit monochrome camera at the Imaging Facility of the Max Planck Institute of Biochemistry, Martinsried.

ACCESSION NUMBERS

The accession number for ChIP-seq data reported in this paper is GEO: GSE76949.

SUPPLEMENTAL INFORMATION

Supplemental Information includes Supplemental Experimental Procedures, six figures, and one table and can be found with this article online at http://dx.doi.org/10.1016/j.celrep.2016.01.066.

AUTHOR CONTRIBUTIONS

Strain Construction, A.M., L.W., and F.B.; Live-Cell Imaging, A.M. and L.W.; ChIP-qPCR, A.M. and L.W.; ChIP-Seq Experiments, A.M.; Cys Cross-Linking Experiments, F.B.; Exploratory ChIP-qPCR Experiments, A.A.; Mapping of the Smc Coiled Coil Register and Protein Purification, M.-L.D.-D; Conception and Interpretation of Experiments, A.M., F.B., and S.G.; Manuscript Preparation, A.M., F.B., L.W., and S.G.

ACKNOWLEDGMENTS

Next-generation sequencing (NGS) library preparation and sequencing was performed at the Max Planck-Genome-Centre Cologne. We thank Thomas Gerland and Verena Kuttenberger for strain construction and exploratory experiments. We are grateful to Stefan Jentsch for sharing equipment and the Max Planck Institute of Biochemistry core facility for SEC-MALS analysis. This work was supported by a European Research Council Starting Grant to S.G. (DiseNtAngle 260853) and the Max Planck Society. M.-L.D.-D. is supported by an EMBO long-term fellowship.

Received: September 23, 2015
Revised: December 22, 2015
Accepted: January 21, 2016
Published: February 18, 2016

REFERENCES

Alipour, E., and Marko, J.F. (2012). Self-organization of domain structures by DNA-loop-extruding enzymes. Nucleic Acids Res. *40*, 11202–11212.

Badrinarayanan, A., Reyes-Lamothe, R., Uphoff, S., Leake, M.C., and Sherratt, D.J. (2012). In vivo architecture and action of bacterial structural maintenance of chromosome proteins. Science *338*, 528–531.

Britton, R.A., Lin, D.C., and Grossman, A.D. (1998). Characterization of a prokaryotic SMC protein involved in chromosome partitioning. Genes Dev. *12*, 1254–1259.

Bürmann, F., and Gruber, S. (2015). SMC condensin: promoting cohesion of replicon arms. Nat. Struct. Mol. Biol. *22*, 653–655.

Bürmann, F., Shin, H.C., Basquin, J., Soh, Y.M., Giménez-Oya, V., Kim, Y.G., Oh, B.H., and Gruber, S. (2013). An asymmetric SMC-kleisin bridge in prokaryotic condensin. Nat. Struct. Mol. Biol. *20*, 371–379.

Cuylen, S., Metz, J., and Haering, C.H. (2011). Condensin structures chromosomal DNA through topological links. Nat. Struct. Mol. Biol. *18*, 894–901.

Danilova, O., Reyes-Lamothe, R., Pinskaya, M., Sherratt, D., and Possoz, C. (2007). MukB colocalizes with the oriC region and is required for organization of the two Escherichia coli chromosome arms into separate cell halves. Mol. Microbiol. *65*, 1485–1492.

Gligoris, T.G., Scheinost, J.C., Bürmann, F., Petela, N., Chan, K.L., Uluocak, P., Beckouët, F., Gruber, S., Nasmyth, K., and Löwe, J. (2014). Closing the cohesin ring: structure and function of its Smc3-kleisin interface. Science *346*, 963–967.

Graumann, P.L., Losick, R., and Strunnikov, A.V. (1998). Subcellular localization of Bacillus subtilis SMC, a protein involved in chromosome condensation and segregation. J. Bacteriol. *180*, 5749–5755.

Gruber, S., and Errington, J. (2009). Recruitment of condensin to replication origin regions by ParB/SpoOJ promotes chromosome segregation in B. subtilis. Cell *137*, 685–696.

Gruber, S., Haering, C.H., and Nasmyth, K. (2003). Chromosomal cohesin forms a ring. Cell *112*, 765–777.

Gruber, S., Veening, J.W., Bach, J., Blettinger, M., Bramkamp, M., and Errington, J. (2014). Interlinked sister chromosomes arise in the absence of condensin during fast replication in B. subtilis. Curr. Biol. *24*, 293–298.

Haering, C.H., Löwe, J., Hochwagen, A., and Nasmyth, K. (2002). Molecular architecture of SMC proteins and the yeast cohesin complex. Mol. Cell *9*, 773–788.

Haering, C.H., Schoffnegger, D., Nishino, T., Helmhart, W., Nasmyth, K., and Löwe, J. (2004). Structure and stability of cohesin's Smc1-kleisin interaction. Mol. Cell *15*, 951–964.

Hinshaw, S.M., Makrantoni, V., Kerr, A., Marston, A.L., and Harrison, S.C. (2015). Structural evidence for Scc4-dependent localization of cohesin loading. eLife *4*, e06057.

Hirano, M., and Hirano, T. (2002). Hinge-mediated dimerization of SMC protein is essential for its dynamic interaction with DNA. EMBO J. *21*, 5733–5744.

Hirano, M., and Hirano, T. (2004). Positive and negative regulation of SMC-DNA interactions by ATP and accessory proteins. EMBO J. *23*, 2664–2673.

Hirano, M., and Hirano, T. (2006). Opening closed arms: long-distance activation of SMC ATPase by hinge-DNA interactions. Mol. Cell *21*, 175–186.

Hirano, M., Anderson, D.E., Erickson, H.P., and Hirano, T. (2001). Bimodal activation of SMC ATPase by intra- and inter-molecular interactions. EMBO J. *20*, 3238–3250.

Houlard, M., Godwin, J., Metson, J., Lee, J., Hirano, T., and Nasmyth, K. (2015). Condensin confers the longitudinal rigidity of chromosomes. Nat. Cell Biol. *17*, 771–781.

Hu, B., Itoh, T., Mishra, A., Katoh, Y., Chan, K.L., Upcher, W., Godlee, C., Roig, M.B., Shirahige, K., and Nasmyth, K. (2011). ATP hydrolysis is required for relocating cohesin from sites occupied by its Scc2/4 loading complex. Curr. Biol. *21*, 12–24.

Kamada, K., Miyata, M., and Hirano, T. (2013). Molecular basis of SMC ATPase activation: role of internal structural changes of the regulatory subcomplex ScpAB. Structure *21*, 581–594.

Kleine Borgmann, L.A., Ries, J., Ewers, H., Ulbrich, M.H., and Graumann, P.L. (2013). The bacterial SMC complex displays two distinct modes of interaction with the chromosome. Cell Rep. *3*, 1483–1492.

Lammens, A., Schele, A., and Hopfner, K.P. (2004). Structural biochemistry of ATP-driven dimerization and DNA-stimulated activation of SMC ATPases. Curr. Biol. *14*, 1778–1782.

Le, T.B., Imakaev, M.V., Mirny, L.A., and Laub, M.T. (2013). High-resolution mapping of the spatial organization of a bacterial chromosome. Science *342*, 731–734.

Lindow, J.C., Kuwano, M., Moriya, S., and Grossman, A.D. (2002). Subcellular localization of the Bacillus subtilis structural maintenance of chromosomes (SMC) protein. Mol. Microbiol. *46*, 997–1009.

Marbouty, M., Cournac, A., Flot, J.F., Marie-Nelly, H., Mozziconacci, J., and Koszul, R. (2014). Metagenomic chromosome conformation capture (meta3C) unveils the diversity of chromosome organization in microorganisms. eLife *3*, e03318.

Marbouty, M., Le Gall, A., Cattoni, D.I., Cournac, A., Koh, A., Fiche, J.B., Mozziconacci, J., Murray, H., Koszul, R., and Nollmann, M. (2015). Condensin- and replication-mediated bacterial chromosome folding and origin condensation revealed by Hi-C and super-resolution imaging. Mol. Cell *59*, 588–602.

Mascarenhas, J., Soppa, J., Strunnikov, A.V., and Graumann, P.L. (2002). Cell cycle-dependent localization of two novel prokaryotic chromosome segregation and condensation proteins in Bacillus subtilis that interact with SMC protein. EMBO J. *21*, 3108–3118.

Mascarenhas, J., Volkov, A.V., Rinn, C., Schiener, J., Guckenberger, R., and Graumann, P.L. (2005). Dynamic assembly, localization and proteolysis of the Bacillus subtilis SMC complex. BMC Cell Biol. *6*, 28.

Melby, T.E., Ciampaglio, C.N., Briscoe, G., and Erickson, H.P. (1998). The symmetrical structure of structural maintenance of chromosomes (SMC) and MukB proteins: long, antiparallel coiled coils, folded at a flexible hinge. J. Cell Biol. *142*, 1595–1604.

Minnen, A., Attaiech, L., Thon, M., Gruber, S., and Veening, J.W. (2011). SMC is recruited to oriC by ParB and promotes chromosome segregation in Streptococcus pneumoniae. Mol. Microbiol. *81*, 676–688.

Moriya, S., Tsujikawa, E., Hassan, A.K., Asai, K., Kodama, T., and Ogasawara, N. (1998). A Bacillus subtilis gene-encoding protein homologous to eukaryotic SMC motor protein is necessary for chromosome partition. Mol. Microbiol. *29*, 179–187.

Nasmyth, K. (2001). Disseminating the genome: joining, resolving, and separating sister chromatids during mitosis and meiosis. Annu. Rev. Genet. *35*, 673–745.

Schleiffer, A., Kaitna, S., Maurer-Stroh, S., Glotzer, M., Nasmyth, K., and Eisenhaber, F. (2003). Kleisins: a superfamily of bacterial and eukaryotic SMC protein partners. Mol. Cell *11*, 571–575.

Schwartz, M.A., and Shapiro, L. (2011). An SMC ATPase mutant disrupts chromosome segregation in Caulobacter. Mol. Microbiol. *82*, 1359–1374.

Shintomi, K., Takahashi, T.S., and Hirano, T. (2015). Reconstitution of mitotic chromatids with a minimum set of purified factors. Nat. Cell Biol. *17*, 1014–1023.

Soh, Y.M., Bürmann, F., Shin, H.C., Oda, T., Jin, K.S., Toseland, C.P., Kim, C., Lee, H., Kim, S.J., Kong, M.S., et al. (2015). Molecular basis for SMC rod formation and its dissolution upon DNA binding. Mol. Cell *57*, 290–303.

Soppa, J., Kobayashi, K., Noirot-Gros, M.F., Oesterhelt, D., Ehrlich, S.D., Dervyn, E., Ogasawara, N., and Moriya, S. (2002). Discovery of two novel families of proteins that are proposed to interact with prokaryotic SMC proteins, and characterization of the Bacillus subtilis family members ScpA and ScpB. Mol. Microbiol. *45*, 59–71.

Sullivan, N.L., Marquis, K.A., and Rudner, D.Z. (2009). Recruitment of SMC by ParB-parS organizes the origin region and promotes efficient chromosome segregation. Cell *137*, 697–707.

Umbarger, M.A., Toro, E., Wright, M.A., Porreca, G.J., Baù, D., Hong, S.H., Fero, M.J., Zhu, L.J., Marti-Renom, M.A., McAdams, H.H., et al. (2011). The three-dimensional architecture of a bacterial genome and its alteration by genetic perturbation. Mol. Cell *44*, 252–264.

Vallet-Gely, I., and Boccard, F. (2013). Chromosomal organization and segregation in Pseudomonas aeruginosa. PLoS Genet. *9*, e1003492.

Please cite this article in press as: Minnen et al., Control of Smc Coiled Coil Architecture by the ATPase Heads Facilitates Targeting to Chromosomal ParB/*parS* and Release onto Flanking DNA, Cell Reports (2016), http://dx.doi.org/10.1016/j.celrep.2016.01.066

Waldman, V.M., Stanage, T.H., Mims, A., Norden, I.S., and Oakley, M.G. (2015). Structural mapping of the coiled-coil domain of a bacterial condensin and comparative analyses across all domains of life suggest conserved features of SMC proteins. Proteins *83*, 1027–1045.

Wang, X., Tang, O.W., Riley, E.P., and Rudner, D.Z. (2014). The SMC condensin complex is required for origin segregation in Bacillus subtilis. Curr. Biol. *24*, 287–292.

Wang, X., Le, T.B., Lajoie, B.R., Dekker, J., Laub, M.T., and Rudner, D.Z. (2015). Condensin promotes the juxtaposition of DNA flanking its loading site in Bacillus subtilis. Genes Dev. *29*, 1661–1675.

Wilhelm, L., Bürmann, F., Minnen, A., Shin, H.C., Toseland, C.P., Oh, B.H., and Gruber, S. (2015). SMC condensin entraps chromosomal DNA by an ATP hydrolysis dependent loading mechanism in Bacillus subtilis. eLife *4*, 4.

Cell Reports, Volume *14*

Supplemental Information

Control of Smc Coiled Coil Architecture by the ATPase Heads Facilitates Targeting to Chromosomal ParB/*parS* and Release onto Flanking DNA

Anita Minnen, Frank Bürmann, Larissa Wilhelm, Anna Anchimiuk, Marie-Laure Diebold-Durand, and Stephan Gruber

I.) Supplemental Data

Figure S1 Expression, functionality and localization of ATPase mutant Smc proteins. Related to Figure 1.

(A) Colony formation assay using strains BSG1002, 1007, 1045, 1047, 1046, 1008 and 1083. Notably, Smc(EQ) mutant cells form colonies on minimal medium slightly more slowly than wild type or *smc* deletion mutants, suggesting that the mutant protein is mildly toxic when normal Smc function is lacking (Figure S1C, D) (Schwartz and Shapiro, 2011). The slow growth is likely due to a defect in replication origin segregation (Gruber et al., 2014; Schwartz and Shapiro, 2011; Wang et al., 2014), which provides a plausible explanation for the lower number of (replication origin-proximal) Smc foci in Smc(EQ) cells (see Figure S1H). (B) Protein extracts stained by Commassie Brilliant Blue. Immunoblotting of identical protein samples is shown in Figure 1B. (C) Same as in (A) with strains BSG1002, 1007, 1008, 1067, 1068 and 1855. (D) Immunoblotting of extracts from strains BSG1002, 1067, 1855, 1857, 1856, 1068, 1881, 1378, 1413, 1677, 1662, 1799 and 1798 with anti-GFP antiserum (top panel). SDS-PAGE of identical extracts stained by Commassie Brilliant Blue (bottom panel). (E) Immunoblotting against Smc protein using strains BSG1007, 1067, 1002, 1045, 1046, 1008, 2050, 2051. (F) Colony formation assay using strains BSG1002, 1007, 1045, 1046, 1008, 2050 and 2051. (G) ChIP-qPCR using anti-Smc antiserum on strains BSG1002, 1008, 1045, 1046, 2050 and 2051. (H) Quantification of Smc-GFP foci in strains shown in Figure 1C. Number of foci is displayed per unit cell length (µm). Standard deviation is derived from four different fields of view for each genotype. 'n' denotes the total number of individual cells counted.

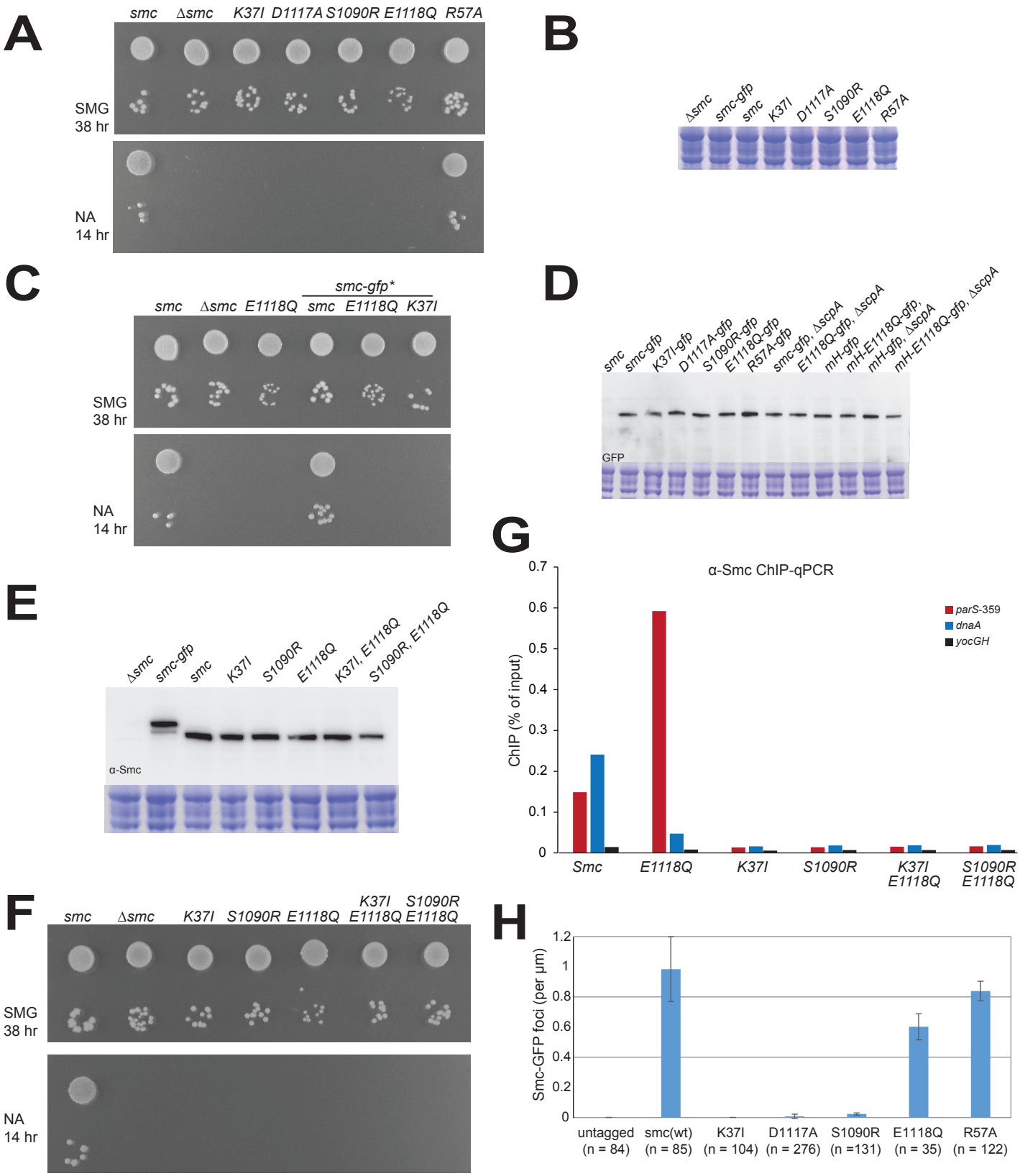
A
smc
Δsmc
K37I
D1117A
S1090R
E1118Q
R57A
SMG
38 hr
NA
14 hr
B
Δsmc
smc-gfp
smc
K37I
D1117A
S1090R
E1118Q
R57A
C
smc-gfp*
smc
Δsmc
E1118Q
smc
E1118Q
K37I
SMG
38 hr
NA
14 hr
D
smc
smc-gfp
K37I-gfp
D1117A-gfp
S1090R-gfp
E1118Q-gfp
R57A-gfp
smc-gfp, ΔscpA
E1118Q-gfp, ΔscpA
mH-gfp
mH-E1118Q-gfp, ΔscpA
mH-gfp, ΔscpA
mH-E1118Q-gfp, ΔscpA
GFP
E
Δsmc
smc-gfp
smc
K37I
S1090R
E1118Q
K37I, E1118Q
S1090R, E1118Q
α-Smc
G
α-Smc ChIP-qPCR
ChIP (% of input)
0.7
0.6
0.5
0.4
0.3
0.2
0.1
0
parS-359
dnaA
yocGH
Smc
E1118Q
K37I
S1090R
K37I E1118Q
S1090R E1118Q
F
smc
Δsmc
K37I
S1090R
E1118Q
K37I E1118Q
S1090R E1118Q
SMG
38 hr
NA
14 hr
H
Smc-GFP foci (per μm)
1.2
1
0.8
0.6
0.4
0.2
0
untagged (n = 84)
smc(wt) (n = 85)
K37I (n = 104)
D1117A (n = 276)
S1090R (n =131)
E1118Q (n = 35)
R57A (n = 122)

Figure S1

Figure S2 Smc and ScpB ChIP-Seq in Smc and Smc(EQ) cells. Related to Figure 2.
(A) ChIP-Seq analysis of BSG1002 and 1008 using anti-Smc antiserum. Number of reads in 1 kb windows at 100bp intervals are shown for input (IN) and ChIP (IP) samples without prior normalization for input material. Normalized data of the same experiment is shown in Figure 2A and 2C. (B) ChIP-Seq analysis of strains BSG1470 and BSG1472 using anti-ScpB antiserum. Data analysis and display as in (A). (C) Whole-genome ChIP-Seq profile for anti-ScpB ChIP (on strain BSG1470), (also shown in Fgiure 7B; same experiment as in Figure S2B). Sequencing reads are put into 5 kb bins and normalized for input DNA. Please note the generally high degree of similarity between anti-Smc (Figure 2C) and anti-ScpB ChIP-Seq profiles with the ScpB profile possibly displaying a steeper gradient from the replicaton origin to the terminus (Kleine Borgmann et al., 2013). (D) Localization of Smc, Smc(S1090R) and Smc(E1118Q) to sites located on the chromosome arm analyzed by ChIP-qPCR using strains BSG1002, BSG1046 and BSG1008. Mean and standard deviation are calculated from three replicate experiments. Boxed insert displays results from the same experiment with “background” correction by subtraction of ChIP obtained with Smc(S1090R).

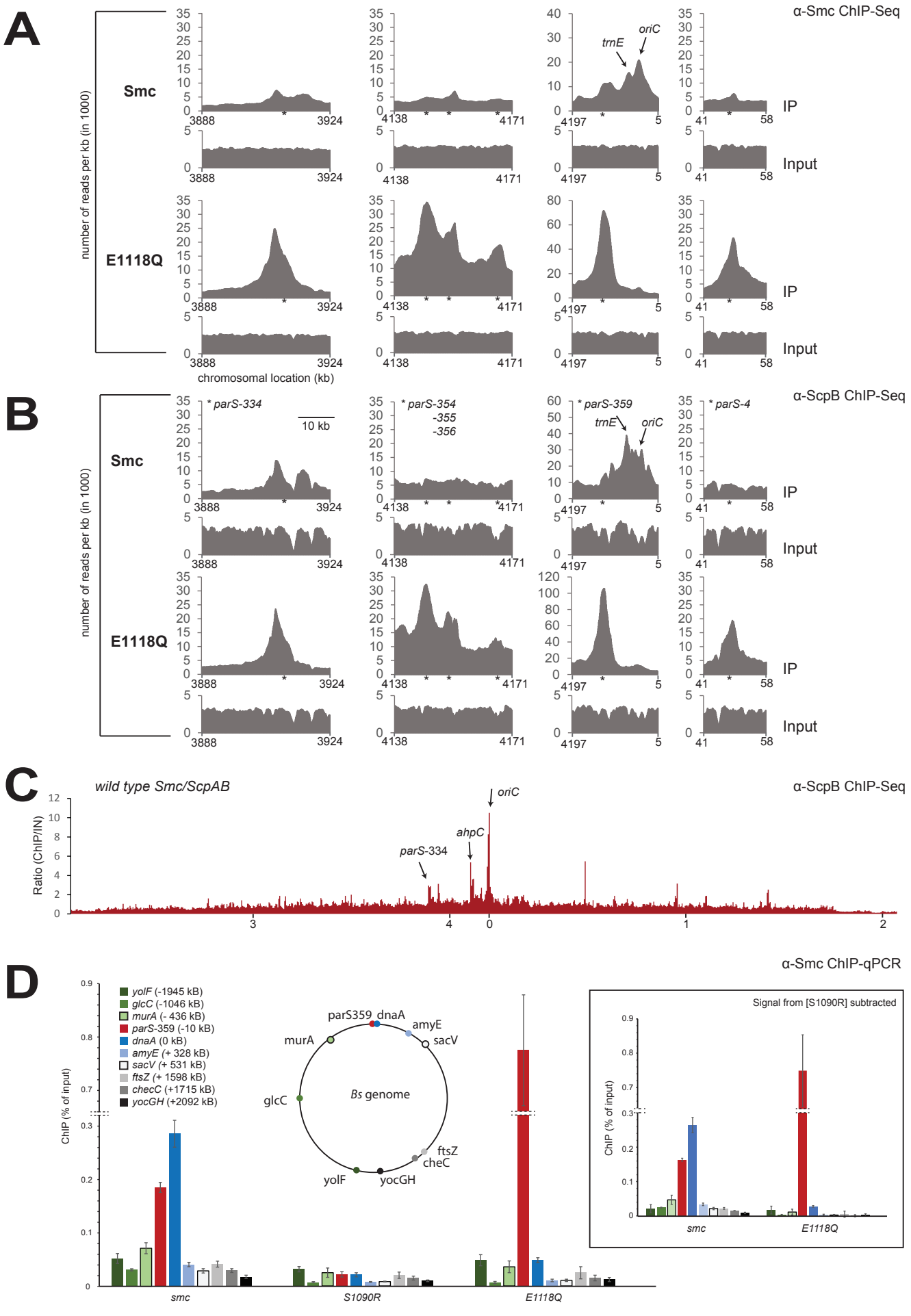
A
α-Smc ChIP-Seq
Smc
E1118Q
IP
Input
number of reads per kb (in 1000)
chromosomal location (kb)
trnE
oriC
B
α-ScpB ChIP-Seq
* parS-334
10 kb
* parS-354
-355
-356
* parS-359
* parS-4
C
wild type Smc/ScpAB
α-ScpB ChIP-Seq
Ratio (ChIP/IN)
parS-334
ahpC
oriC
D
α-Smc ChIP-qPCR
yolF (-1945 kB)
glcC (-1046 kB)
murA (- 436 kB)
parS-359 (-10 kB)
dnaA (0 kB)
amyE (+ 328 kB)
sacV (+ 531 kB)
ftsZ (+ 1598 kB)
checC (+1715 kB)
yocGH (+2092 kB)
ChIP (% of input)
parS359 dnaA
amyE
sacV
murA
glcC
Bs genome
ftsZ
cheC
yolF
yocGH
smc
S1090R
E1118Q
Signal from [S1090R] subtracted

Figure S2

Figure S3 Dimerization at the Smc hinge determines localization of Smc/ScpAB to *parS*. Related to Figure 3.

(A) Immunoblotting of cell extracts from strains BSG1007, 1067, 1002, 1051, 1406, 1052, 1387, 1890, 1893, 1889, 1891 and 1892 using anti-Smc antiserum. (B) Colony formation *Bs* strains BSG1007, 1008, 1889, 1892 and 1891 on minimal medium (SMG). (C) The hinge mutation (GGGG->AAAA) blocks dimerization of headless Smc protein (*Bs*SmcH-CC300). 40 µg of purified proteins was injected onto a gel filtration column and analyzed by multi-angle light scattering (SEC-MALS). Absorbance (at A_{280}) and light scattering is shown for wild-type and hinge mutant *Bs*SmcH-CC300 (curves in red and blue colours, respectively). (D) Analysis of the major peak (in A_{280} absorbance) in SEC-MALS (as in C) of wild-type and hinge-mutant *Bs*SmcH-CC300 indicates the existence of largely dimeric and monomeric protein species, respectively. (E) Immunoblotting of cell extracts from strains BSG1007, 1067, 1002, 1890, 1893, 1892, 1624, 1621 and 1620 using anti-Smc antiserum. (F) Colony formation of strains BSG1007, 1893, 1624, 1621, 1623 and 1620 on minimal medium (SMG). (G) Quantification of Smc-GFP foci in strains shown in Figure 3D. Number of foci is displayed per unit cell length (µm). Standard deviation is derived from four different fields of view for each genotype. 'n' denotes the total number of individual cells counted. (H) ChIP-qPCR analysis of strains BSG1893, 1892, 2144-2147 grown in SMG medium with anti-Smc antiserum.

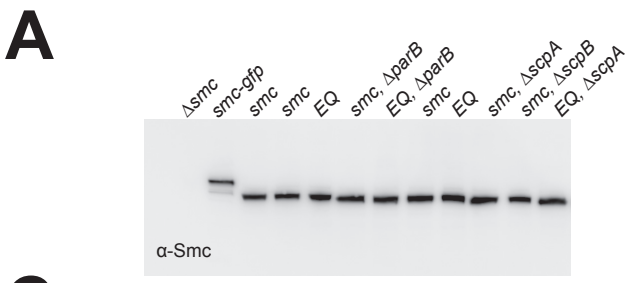

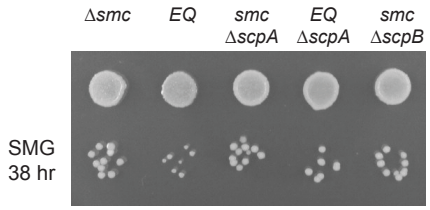

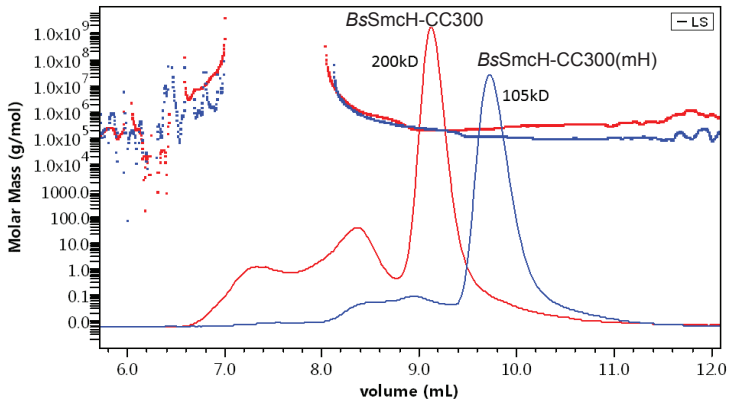

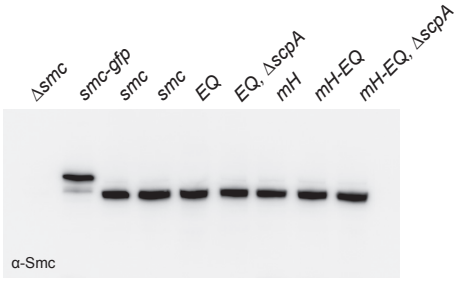

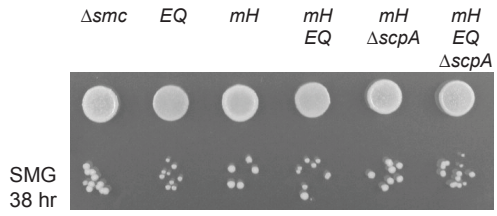

D

	BsSmcH-CC300	BsSmcH-CC300(mH)
Peak analysis (ml)	8.836-9.809	9.404-10.993
Masses		
Injected mass	40µg	40µg
Calculated mass	25.87µg	48.55µg
Mass recovery	64.7%	121.4%
Mass fraction	82.3%	89.1%
Molar mass moments		
Mw	205816.77g/mol	106838.13g/mol
Polydispersity		
Mw/Mn	1.003	1.004
Rms radius moments		
Rz	19.7nm	14.7nm

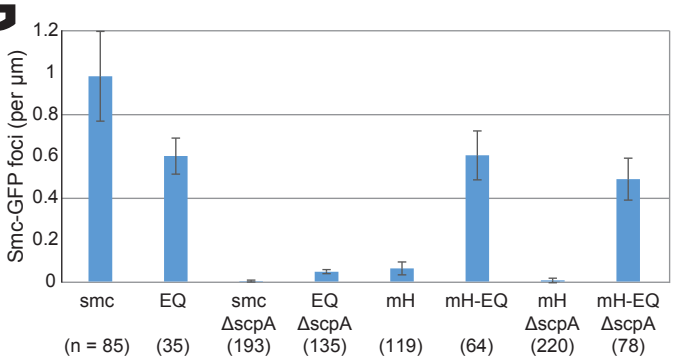

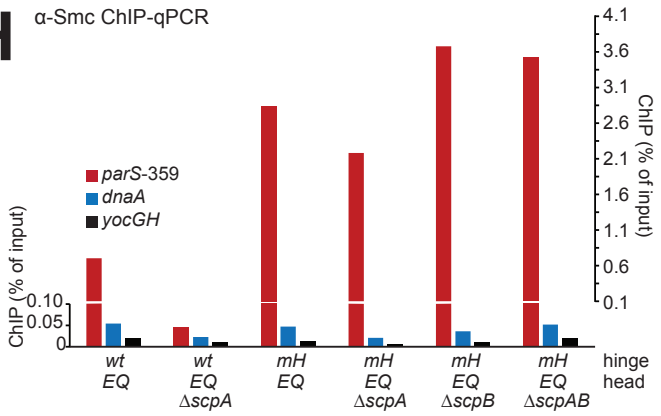

Figure S3

Figure S4 Smc(K1151C) –the reporter for head engagement– is functional. Related to Figure 4.
(A) Colony formation of strains BSG1002, 1007, 1360 and 1457 on minimal medium (SMG) and nutrient rich medium (NA). (B) Cross-linking of Smc(K1151C) in BSG1607, 1488, 1512 and 1513 with BMOE. Mean values and standard deviation from triplicate experiments are shown.

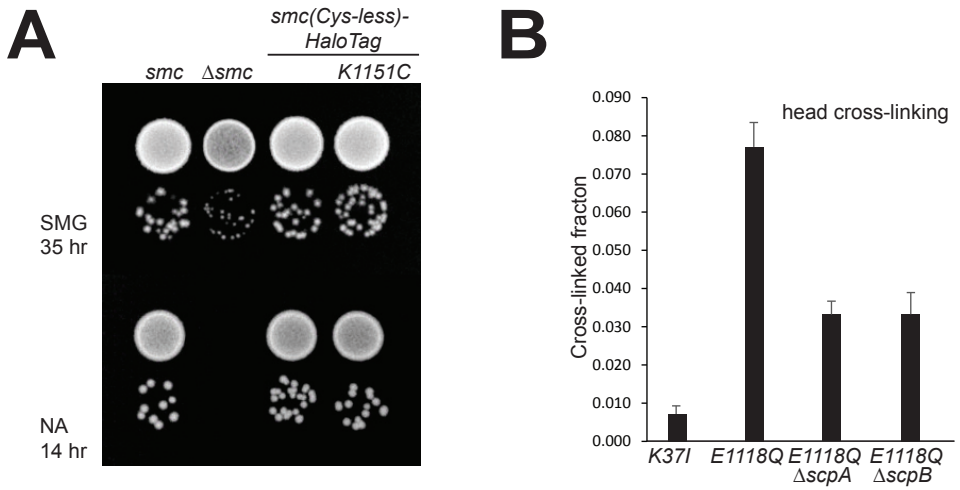
A
smc(Cys-less)-HaloTag
smc
Δsmc
K1151C
SMG 35 hr
NA 14 hr
B
head cross-linking
Cross-linked fracton
0.090
0.080
0.070
0.060
0.050
0.040
0.030
0.020
0.010
0.000
K37I
E1118Q
E1118Q ΔscpA
E1118Q ΔscpB

Figure S4

Figure S5 Expression and functionality of hinge-less Smc protein. Related to Figure 5.
(A) Immunoblotting against the TAP tag on Smc in cell extracts from strains BSG1002, 1016, 1475, 1691, 1896, 1671, 1780, 1672, 1895, 1689 and 1779. Commassie staining of the same extracts is shown in the bottom panel. (B) Colony formation assay using strains BSG1007, 1008, 1626, 1619, 1896 and 1780. (C) Same as in (B) with strains BSG1002, 1007, 1008, 1520, 1689 and 1779. (D) Exemplary image of the SDS-PAGE analysis of disulfide cross-linked *Bs*SmcH-CC300 samples harboring pairs of cysteines as annotated. (E) Quantification of intra- and inter-molecular disulfide formation (after 4 hr incubation) from Commassie stained SDS-PAGE gels for 16 pairs of cysteine mutants. (F) Schematic view of the folding of the Smc coiled coil. Anchor points setting the register of the Smc coiled coils – established by *in vitro* disulfide formation (see D and E)– are given as dashed lines connecting N- and C-terminal helix. Disruptions in the coiled coil register were detected by Marcoil prediction. The length of extra sequences in the C-terminal coiled coil as given by the experimentally determined coiled coil register are indicated at the corresponding positions. Regions relevant for the targeting of mini-Smc to *parS* are highlighted by labels in red colours.

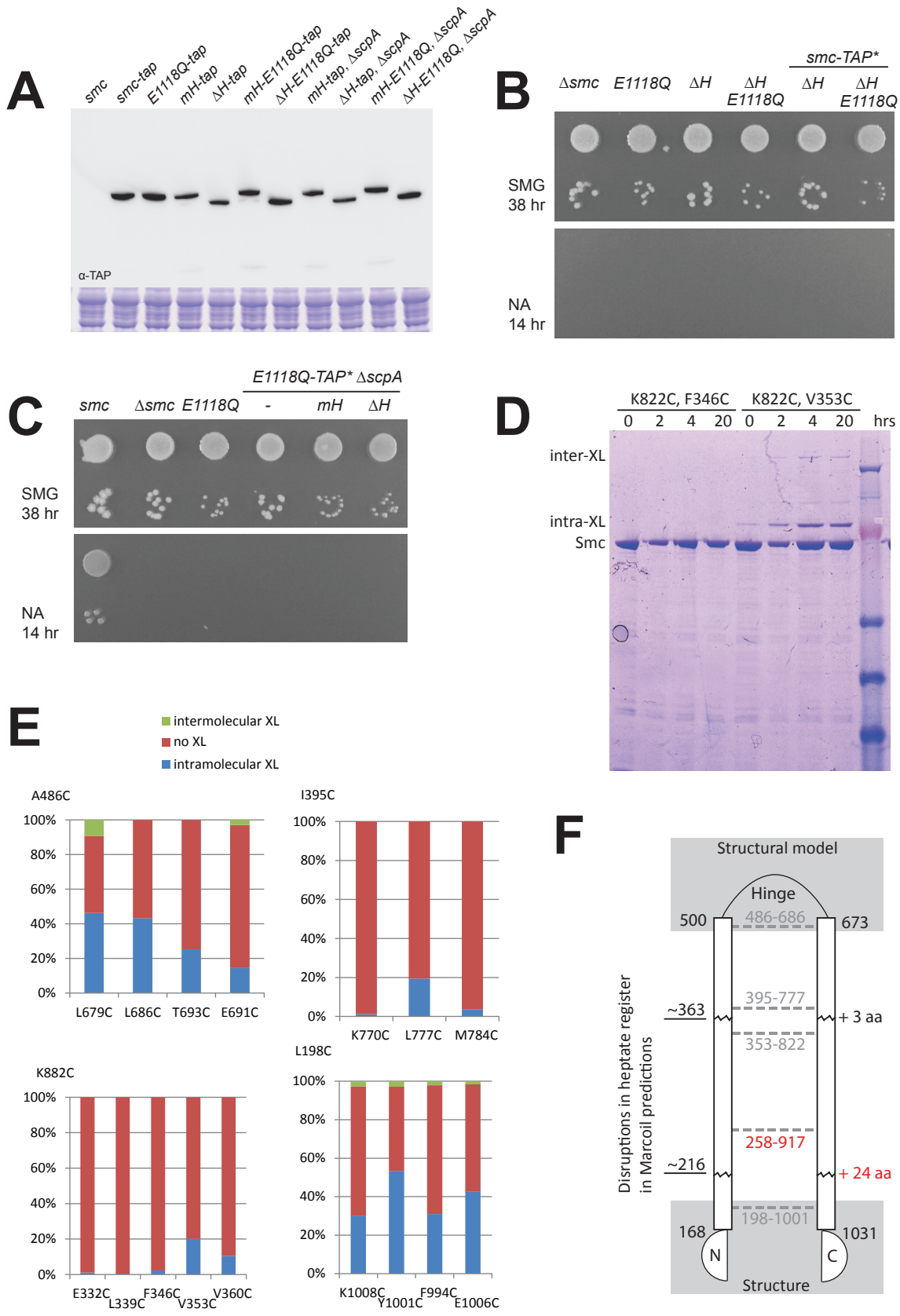
A
smc
smc-tap
E1118Q-tap
mH-tap
ΔH-tap
mH-E1118Q-tap
ΔH-E1118Q-tap
mH-tap, ΔscpA
ΔH-tap, ΔscpA
mH-E1118Q, ΔscpA
ΔH-E1118Q, ΔscpA
α-TAP
B
Δsmc
E1118Q
ΔH
ΔH E1118Q
smc-TAP*
ΔH
ΔH E1118Q
SMG 38 hr
NA 14 hr
C
E1118Q-TAP* ΔscpA
smc
Δsmc
E1118Q
-
mH
ΔH
SMG 38 hr
NA 14 hr
D
K822C, F346C
K822C, V353C
0 2 4 20 0 2 4 20 hrs
inter-XL
intra-XL
Smc
E
intermolecular XL
no XL
intramolecular XL
A486C
100%
80%
60%
40%
20%
0%
L679C L686C T693C E691C
I395C
K770C L777C M784C
K882C
E332C L339C F346C V353C V360C
L198C
K1008C Y1001C F994C E1006C
F
Structural model
Hinge
500
486-686
673
~363
395-777
+ 3 aa
353-822
258-917
~216
+ 24 aa
198-1001
168
1031
N
C
Structure
Disruptions in heptate register in Marcoil predictions

Figure S5

Figure S6 ChIP-Seq of Smc(EQ) to an ectopic *parS* site. Related to Figure 6.
Smc(EQ) is efficiently targeted to *parS-amyE*. ChIP-Seq analysis of BSG1471 (top panel) and BSG1008 (bottom panel) using anti-Smc antiserum. ChIP eluate sequence reads were mapped to 5 kb bins and normalized for input DNA. Please note that Smc(EQ) localization to endogenous parS sites is decreased by the presence of an extra *parS* site, being consistent with a titration effect. The bottom panel is identical to the bottom panel of Figure 2C.

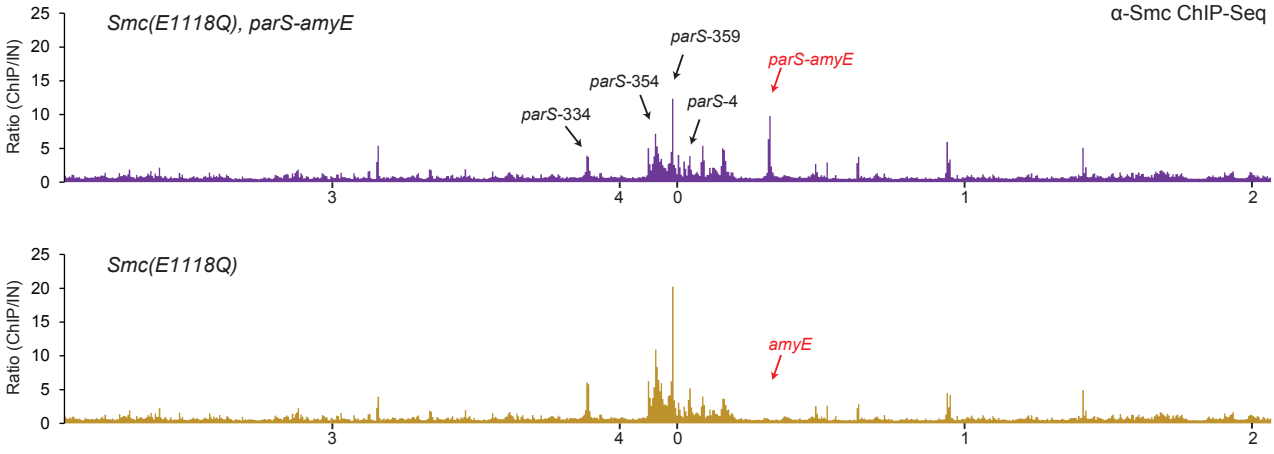
Smc(E1118Q), parS-amyE
α-Smc ChIP-Seq
Ratio (ChIP/IN)
parS-359
parS-amyE
parS-354
parS-4
parS-334
Smc(E1118Q)
amyE
3
4
0
1
2

Figure S6

II.) Supplemental Table

Supplemental Table 1 Genotypes

All strains are derivatives of *Bacillus subtilis* 1A700 provided by the BGSC (*Bacillus* Genetic Stock Center). All strains are auxotrophic for tryptophan (*trpC2*).

BSG1002	smc ftsY::ermB
BSG1007	Δsmc ftsY::ermB
BSG1008	smc(E1118Q) ftsY::ermB
BSG1016	smc-TAP ftsY::ermB
BSG1045	smc(K37I) ftsY::ermB
BSG1046	smc(S1090R) ftsY::ermB
BSG1047	smc(D1117A) ftsY::ermB
BSG1051	smc ftsY::ermB, parAB::kanR
BSG1052	smc ftsY::ermB, ΔparB::kanR
BSG1067	smc-mGFPmut1 ftsY::ermB
BSG1068	smc(E1118Q)-mGFP1mut1 ftsY::ermB
BSG1083	smc(R57A) ftsY::ermB
BSG1360	smc(C119S, C437S, C826S, C1114S)-TEV-His12-HaloTag(C61V, C262A) ftsY::ermB
BSG1378	smc-mGFPmut1 ftsY::ermB, specR::ΔscpA
BSG1387	smc(E1118Q) ftsY::ermB, ΔparB::kanR
BSG1406	smc(E1118Q) ftsY::ermB, parAB::kanR
BSG1413	smc(E1118Q)-mGFP1mut1 ftsY::ermB, specR::ΔscpA
BSG1457	smc(C119S, C437S, C826S, C1114S, K1151C)-TEV-His12-HaloTag(C61V, C262A) ftsY::ermB
BSG1469	smc ftsY::ermB, ΔamyE::parS-359::cat
BSG1470	smc ftsY::ermB, ΔamyE::mtparS-359::cat
BSG1471	smc(E1118Q) ftsY::ermB, ΔamyE::parS-359::cat
BSG1472	smc(E1118Q) ftsY::ermB, ΔamyE::mtparS-359::cat
BSG1475	smc(E1118Q)-TAP ftsY::ermB
BSG1488	smc(C119S, C437S, C826S, C1114S, K1151C, E1118Q)-TEV-His12-HaloTag(C61V, C262A) ftsY::ermB
BSG1509	smc(C119S, C437S, C826S, C1114S, K1151C)-TEV-His12-HaloTag(C61V, C262A) ftsY::ermB, specR::ΔscpA
BSG1512	smc(C119S, C437S, C826S, C1114S, K1151C, E1118Q)-TEV-His12-HaloTag(C61V, C262A) ftsY::ermB, specR::ΔscpA
BSG1513	smc(C119S, C437S, C826S, C1114S, K1151C, E1118Q)-TEV-His12-HaloTag(C61V, C262A) ftsY::ermB, specR::scpA ΔscpB
BSG1520	smc(E1118Q)-TAP ftsY::ermB, specR::ΔscpA
BSG1547	smc(G657A, G658A, G662A, G663A, E1118Q)-ftsY::ermB
BSG1597	smc(C119S, C437S, G657A, G658A, G662A, G663A, C826S, C1114S, K1151C)-TEV-His12-HaloTag(C61V, C262A) ftsY::ermB
BSG1598	smc(C119S, C437S, G657A, G658A, G662A, G663A, C826S, C1114S, E1118Q, K1151C)-TEV-His12-HaloTag(C61V, C262A) ftsY::ermB
BSG1607	smc(K37I, C119S, C437S, C826S, C1114S, K1151C)-TEV-His12-HaloTag(C61V, C262A) ftsY::ermB
BSG1619	rncS smc(1-499 GGGSGGGSGGG 674-1186, E1118Q) ftsY::ermB
BSG1620	smc(G657A, G658A, G662A, G663A, E1118Q)-ftsY::ermB, specR::ΔscpA
BSG1621	smc(G657A, G658A, G662A, G663A, E1118Q)-ftsY::ermB, specR::scpAB
BSG1624	smc(G657A, G658A, G662A, G663A) ftsY::ermB, specR::scpAB
BSG1626	rncS smc(1-499 GGGSGGGSGGG 674-1186) ftsY::ermB
BSG1662	smc(G657A, G658A, G662A, G663A, E1118Q)-mGFP-ftsY::ermB
BSG1671	smc(G657A, G658A, G662A, G663A, E1118Q)-TAP-ftsY::ermB, specR::scpAB
BSG1672	smc(G657A, G658A, G662A, G663A)-TAP ftsY::ermB, specR::ΔscpA
BSG1677	smc(G657A, G658A, G662A, G663A)-mGFP-ftsY::ermB

BSG1689	smc(G657A, G658A, G662A, G663A, E1118Q)-TAP ftsY::ermB, specR::ΔscpA
BSG1691	smc(G657A, G658A, G662A, G663A)-TAP ftsY::ermB, specR::scpAB
BSG1779	smc(1-499 GGGSGGGSGGG 674-1186, E1118Q)-TAP::ermB, specR::ΔscpA
BSG1780	smc(1-499 GGGSGGGSGGG 674-1186, E1118Q)-TAP::ermB, specR::scpAB
BSG1791	smc(C119S, C437S, G657A, G658A, G662A, G663A, C826S, C1114S, E1118Q, K1151C)-TEV-His12-HaloTag(C61V, C262A) ftsY::ermB, specR::ΔscpA
BSG1798	smc(G657A, G658A, G662A, G663A, E1118Q)-mGFP-ftsY::ermB, specR::ΔscpA
BSG1799	smc(G657A, G658A, G662A, G663A)-mGFP-ftsY::ermB, specR::ΔscpA
BSG1800	smc(C119S, C437S, G657A, G658A, G662A, G663A, C826S, C1114S, K1151C)-TEV-His12-HaloTag(C61V, C262A) ftsY::ermB, specR::ΔscpA
BSG1824	smc(1-199 GGGSGGGSGGG 999-1186, E1118Q)-TAP::ermB, specR::ΔscpA
BSG1825	smc(1-219 GPG 983-1186, E1118Q)-TAP::ermB, specR::ΔscpA
BSG1826	smc(1-243 GGGSGGGSGGG 957-1186, E1118Q)-TAP::ermB, specR::ΔscpA
BSG1827	smc(1-243 GGGSGGGSGGG 943-1186, E1118Q)-TAP::ermB, specR::ΔscpA
BSG1828	smc(1-261 GGGSGGGSGGG 943-1186, E1118Q)-TAP::ermB, specR::ΔscpA
BSG1829	smc(1-261 GGGSGGGSGGG 912-1186, E1118Q)-TAP::ermB, specR::ΔscpA
BSG1830	smc(1-277 GGGSGGGSGGG 922-1186, E1118Q)-TAP::ermB, specR::ΔscpA
BSG1855	smc(K37I)-mGFP1mut1 ftsY::ermB
BSG1856	smc(S1090R)-mGFP1mut1 ftsY::ermB
BSG1857	smc(D1117A)-mGFP1mut1 ftsY::ermB
BSG1871	smc(1-468 GGGSGGGSGGG 705-1186, E1118Q)-TAP::ermB, specR::ΔscpA
BSG1872	smc(1-437 GGGSGGGSGGG 736-1186, E1118Q)-TAP::ermB, specR::ΔscpA
BSG1873	smc(1-315 GGGSGGGSGGG 858-1186, E1118Q)-TAP::ermB, specR::ΔscpA
BSG1874	smc(1-370 GGGSGGGSGGG 803-1186, E1118Q)-TAP::ermB, specR::ΔscpA
BSG1875	smc(1-414 GGGSGGGSGGG 785-1186, E1118Q)-TAP::ermB, specR::ΔscpA
BSG1881	smc(R57A)-mGFP1mut1 ftsY::ermB
BSG1889	smc ftsY::ermB, specR::ΔscpA
BSG1890	smc ftsY::ermB, specR::scpAB
BSG1891	smc ftsY::ermB, specR::scpA ΔscpB
BSG1892	smc(E1118Q) ftsY::ermB, specR::ΔscpA
BSG1893	smc(E1118Q) ftsY::ermB, specR::scpAB
BSG1895	smc(1-499 GGGSGGGSGGG 674-1186)-TAP ftsY::ermB, specR::ΔscpA
BSG1896	smc(1-499 GGGSGGGSGGG 674-1186)-TAP ftsY::ermB, specR::scpAB
BSG1921	smc(C119S, C437S, A715C, C826S, C1114S)-TEV-His12-HaloTag(C61V, C262A) ftsY::ermB
BSG1922	smc(C119S, C437S, A715C, C826S, C1114S, E1118Q)-TEV-His12-HaloTag(C61V, C262A) ftsY::ermB
BSG1923	smc(C119S, C437S, G657A, G658A, G662A, G663A, A715C, C826S, C1114S)-TEV-His12-HaloTag(C61V, C262A) ftsY::ermB
BSG1924	smc(C119S, C437S, G657A, G658A, G662A, G663A, A715C, C826S, C1114S, E1118Q)-TEV-His12-HaloTag(C61V, C262A) ftsY::ermB
BSG1949	smc(C119S, C437S, A715C, C826S, C1114S)-TEV-His12-HaloTag(C61V, C262A) ftsY::ermB, specR::ΔscpA
BSG1950	smc(C119S, C437S, A715C, C826S, C1114S, E1118Q)-TEV-His12-HaloTag(C61V, C262A) ftsY::ermB, specR::ΔscpA
BSG1951	smc(C119S, C437S, G657A, G658A, G662A, G663A, A715C, C826S, C1114S)-TEV-His12-HaloTag(C61V, C262A) ftsY::ermB, specR::ΔscpA
BSG2036	smc(C119S, C437S, G657A, G658A, G662A, G663A, A715C, C826S, C1114S, E1118Q)-TEV-His12-HaloTag(C61V, C262A) ftsY::ermB, specR::ΔscpA
BSG2050	smc(K37I, E1118Q) ftsY::ermB
BSG2051	smc(S1090R, E1118Q) ftsY::ermB
BSG2144	specR::scpAB, smc(G657A, G658A, G662A, G663A, E1118Q)-ftsY::ermB
BSG2145	specR::ΔscpA, smc(G657A, G658A, G662A, G663A, E1118Q)-ftsY::ermB
BSG2146	specR::scpA ΔscpB, smc(G657A, G658A, G662A, G663A, E1118Q)-ftsY::ermB
BSG2147	specR::ΔscpAB, smc(G657A, G658A, G662A, G663A, E1118Q)-ftsY::ermB

III.) Supplemental Experimental Procedures

In vivo expression of Smc proteins tested by immunoblotting

Cells were grown in SMG at 37°C to an OD_{600} of 0.02-0.03, harvested by centrifugation or filtrations and washed once in 2 ml PBSG (PBS + 0.1% glycerol). The OD_{600} was measured and equivalent amount of cells for all samples were taken (0.02 ml*OD_{600}). Cells were resuspended in PBSG, ß-mercaptoethanol was added to a final concentration of 28.6 mM and kept on ice for 3 min. Lysozyme (12.8U/µl final), *Roche Complete* protease inhibitor cocktail and Benzonase (0.4 U/µl; Sigma-Aldrich) were added and the samples were incubated at 37°C for 20 min. NuPage LDS loading dye (final 1x) and DTT (final conc. 100 mM) were added and the samples incubated at 70°C for 10 min. The extracts were loaded on a 4-12% NuPAGE Bis-Tris gel run in MOPS buffer for 50 min at 200 V. Proteins were transferred to a PVDF membrane which was treated with α-Smc, α-GFP (Life Technologies, A6455) or Peroxidase Anti-Peroxidase (PAP). α-Smc and α-GFP blots were treated with ECL Anti-rabbit IgG, HRP-linked whole antibody (from donkey) (GE healthcare). The blots were incubated with Supersignal West Femto (Thermo Scientific) and were imaged in a LAS4000 scanner.

Chromatin immuno-precipitation (ChIP) and qPCR

Cells were grown in SMG medium at 37ºC overnight and diluted to OD_{600} 0.005 in SMG. At OD 0.02-0.03 40 ml of fixing solution (50mM Tris/HCl pH 8.0, 100mM NaCl, 1mM EDTA, 0.5mM EGTA, 11% formaldehyde) was added to 400 ml of culture and incubated at room temperature for 30 minutes. Cells were harvested by centrifugation or filtration and washed in 2 ml ice-cold PBS and OD_{600} was measured. Cells were resuspended in 1 ml TESS (50mM Tris/HCl 7.4, 10mM EDTA, 50mM NaCl, 500mM sucrose) and protoplasted by incubating in 1 ml TESS supplemented with 20mg/ml lysozyme (Sigma) and Roche Complete protease inhibitor cocktail for 30 min at 37°C shaking. Cells were washed once in 1 ml TESS, aliquoted according to the previously measured OD_{600} and stored at -80°C.

One aliquot of fixed cells was resuspended in 2 ml lysis buffer (50mM Hepes/KOH pH 7.5, 140mM NaCl, 1mM EDTA, 1% (v/v) Triton X-100, 0.1% (w/v) sodium deoxycholate, 100mg/ml RNase, *Roche Complete* protease inhibitor cocktail) and transferred to a 5 ml round-bottom tube. The samples were sonicated 3 x 20 sec on a Bandelin Sonoplus with a MS-72 tip at 90% pulse and 35% power output. Lysates were transferred into 2 ml tubes and centrifuged 5 min at 21000g and the supernatant subsequently 10 min at 21000g at 4°C.

200 µl of the cleared lysates was kept separate as the input sample. 50 µl Protein G coupled dynabead (Invitrogen) were incubated with 50 µl antibody serum (α-Smc, α-ScpB or α-ParB generated in rabbit) for at least 1 hr rotating at 4°C. Beads were washed in lysis buffer and added to 800 µl of the cleared lysates. For experiments involving TAP-tagged strains, rabbit IgG coupled to 50 µl magnetic DynaBeads (Epoxy, M-270) (prepared according to the manufacturer's protocol) was added to 800 µl cleared lysates. The beads with cleared lysates were incubated at 4°C rotating for 2-4 hours. Beads were washed once with each of the following buffers, lysis buffer, lysis buffer with high salt (500mM NaCl) and wash buffer (10mM Tris/HCl pH 8.0, 250mM LiCl, 1mM EDTA, 0.5% (w/v) NP-40, 0.5% (w/v) sodium deoxycholate). Beads were resuspended in 520 µl TES (50mM Tris/HCl pH 8.0, 10mM EDTA, 1% SDS), the input samples were combined with 300 µl TES and 20 µl 10% SDS solution and incubated overnight at 65°C shaking. DNA was purified by phenol chloroform extraction and ethanol precipitation. The DNA was dissolved in 100µl TE at 65°C for 20 min and purified on a Qiagen PCR purification column and eluted in 30 µl EB. For qPCR 4 µl of the input DNA (diluted 1:200) and IP samples (diluted 1:20) was used in a 10 µl reaction using 5 µl Takyon no ROX SYBR Mastermix blue dTTP (Eurogentec) and 1 µl primer pair stock solution (3 µM each primer) on a Qiagen Rotor-Gene Q in a 72 well rotor according to manufacturer's instructions. Primer sequences are given in the table below. Curves were analyzed by determining the maximum of the 2nd derivative using the Real-time PCR miner software (http://ewindup.info) (Zhao and Fernald, 2005). ChIP efficiencies were calculated as follows: [(IP/input)*100] for each primer pair.

List of primer pairs for qPCR:

parS-356	STG236	tgaaaagaatgcccatcaca
	STG237	tgcaagcaacaaccctttac
parS-359	STG097	aaaaagtgattgcggagcag
	STG098	agaaccgcatctttcacagg
dnaA	STG199	gatcaatcggggaaagtgtg
	STG200	gtagggcctgtggatttgtg
trnS	STG404	gggttttgacaccttggta
	STG405	aagcaaaaggaaatggctga
cheC	STG396	tttgcatgaactgggcaata
	STG397	tccgaacatgtccaatgaga
yocGH	STG099	tccatatcctcgctcctacg
	STG100	attctgctgatgtgcaatgg

Protein purification and SEC-MALS

Wild-type and hinge mutant *Bs*SmcH-CC300 protein (Smc residues 188-1011) were overexpressed from plasmid pnEA-tH in *E. coli* with an N-terminal HISx6 tag (Diebold et al., 2011). The proteins were purified via a HisTrap column, concentrated by anion-exchange chromatography (MonoQ HiTrap) and eluted from a size exclusion chromatography column (Superdex 200 10/300) in 200mM NaCl, 25mM Tris/HCl pH 7.4 (4°C). Multi-angle light scattering coupled to size exclusion chromatography (SEC-MALS) was performed as described previously (Soh et al., 2015).

Viability spotting assay

Cells were grown in SMG medium overnight into stationary phase, diluted 81-fold and 59049-fold (in 9x steps) and spotted on nutrient agar plates (Oxoid) or SMG agar plates. Plates were incubated at 37°C for ~12 hr on NA or ~36 hr on SMG agar.

Mapping of the *Bs* Smc coiled coil register by disulfide formation

Intramolecular crosslinking reactions for the determination of the coiled coil register were performed essentially as described in (Waldman et al., 2015) using the BsSmcH-CC300 construct (Soh et al., 2015). The protein was expressed from the pnEA-tH plasmid as a His-Tag fusion protein. For each double cysteine mutant, 50mL cultures were set-up. Cells were lysed by sonication and soluble extract was incubated for one hour with 300uL of Talon resin (Clontech). Beads were washed three times with the lysis buffer (200 mM NaCl, 50 mM NaPi pH7.4, 5 mM Imidazole) and then resuspended in the lysis buffer supplemented with 1 mM magnesium chloride. 1uL of benzonase (Roche) was added to the beads that were shaked for 30min at room temperature to remove the bound DNAs. The beads were washed two more times with the lysis buffer and the proteins were eluted with elution buffer 200 mM NaCl, 500 mM Imidazole, 50 mM NaPi pH7.4.

The proteins were then dialyzed against PBS buffer containing 4 mM DTT for 2 hours. For the crosslinking reaction, the protein was diluted to a concentration of 5 µM. The non-crosslinked sample was prepared by adding 1mM of iodoacetamide and heating at 70°C for 10 min. Disulfide formation was set-up by adding one volume of PBS supplemented with 5 mM $NaAsO_2$ (Fluka) to the protein and 100 µM dithio-bisnitrobenzoic acid DTNB (Merck) and 300 µM beta-mercaptoethanol. The reaction was incubated at 4°C under shaking. Samples were taken after 2, 4, 6 and 20h of reaction, and quenched by addition of 10 mM iodoacetamide at 70°C for 10 min.

After addition of non-reducing SDS-Page loading buffer the samples were boiled for 5 min at 95°C and run on a Bis-Tris 4-16% NuPage acrylamide gel (Novex) using MOPS buffer as running buffer for 50 min at 200 V.

IV.) Supplemental References

Diebold, M.L., Fribourg, S., Koch, M., Metzger, T., and Romier, C. (2011). Deciphering correct strategies for multiprotein complex assembly by co-expression: application to complexes as large as the histone octamer. Journal of structural biology *175*, 178-188.

Gruber, S., and Errington, J. (2009). Recruitment of condensin to replication origin regions by ParB/SpoOJ promotes chromosome segregation in B. subtilis. Cell *137*, 685-696.
Gruber, S., Haering, C.H., and Nasmyth, K. (2003). Chromosomal cohesin forms a ring. Cell *112*, 765-777.

Kleine Borgmann, L.A., Ries, J., Ewers, H., Ulbrich, M.H., and Graumann, P.L. (2013). The bacterial SMC complex displays two distinct modes of interaction with the chromosome. Cell reports *3*, 1483-1492.

Schwartz, M.A., and Shapiro, L. (2011). An SMC ATPase mutant disrupts chromosome segregation in Caulobacter. Molecular microbiology *82*, 1359-1374.

Soh, Y.M., Burmann, F., Shin, H.C., Oda, T., Jin, K.S., Toseland, C.P., Kim, C., Lee, H., Kim, S.J., Kong, M.S., *et al.* (2015). Molecular basis for SMC rod formation and its dissolution upon DNA binding. Molecular cell *57*, 290-303.

Waldman, V.M., Stanage, T.H., Mims, A., Norden, I.S., and Oakley, M.G. (2015). Structural mapping of the coiled-coil domain of a bacterial condensin and comparative analyses across all domains of life suggest conserved features of SMC proteins. Proteins *83*, 1027-1045.

Wang, X., Tang, O.W., Riley, E.P., and Rudner, D.Z. (2014). The SMC condensin complex is required for origin segregation in Bacillus subtilis. Current biology : CB *24*, 287-292.